MINISTRY OF EDUCATION AND RESEARCH
National University of Science and Technology POLITEHNICA Bucharest

Doctoral School of Industrial Engineering and Robotics

DOCTORAL THESIS

"RESEARCH ON THE BEHAVIOR TO ELECTRIC RESISTANCE WELDING BY PROJECTION OF THIN ALUMINIZED STEEL COMPONENTS"

PhD. student Eng. Alexandru-Vlăduț F. OPREA

Scientific coordinator

Prof. PhD. Eng. Ionelia VOICULESCU

Bucharest - 2026

THANKS

*The PhD dissertation entitled "***Research on the behavior of electric resistance welding by projection of thin aluminized steel components***" was elaborated and revised under the supervision of the tutoring committee composed of Prof. PhD. Eng. Ionelia Voiculescu, Prof. PhD.Eng. Corneliu Rontescu, Lecturer PhD. Eng. Dumitru Titi Cicic, Assistant professor PhD. Eng. Ana Maria Bogatu, to whom I would like to thank for all the constructive comments and suggestions made during the examinations and scientific reports provided in the doctoral training program.*

On this occasion, I would like to express my recognition and thank to Prof. Ionelia Voiculescu for the professional way in which she coordinated, encouraged and guided me in carrying out the program of experiments, tests and trials during my doctoral training. I also thank Mr. Ass. prof. PhD. Eng. Ion Mihai Vasile, who helped me prepare the samples for metallographic analysis, and Mr. Ass.prof. PhD. Eng. Robert Cătălin Ciocoiu, from the SIM faculty, who helped me carry out the tensile tests.

At the same time, I would like to thank Prof. PhD. Eng. Elena Scutelnicu and Lecturer PhD. Eng. Carmen Cătălina Rusu from the "Dunărea de Jos" University of Galați, for their technical support in preparing the manuscript of the work published in the Annals of the "Dunărea de Jos" University of Galați, Fascicle XII, Welding Equipment and Technology (AWET).

I would like to thank the management of the National University of Science and Technology Politehnica Bucharest and the management of the Doctoral School of Industrial Engineering and Robotics, who created favorable conditions for me to carry out scientific activity, as well as for conducting research, tests, for presenting papers and papers at scientific sessions organized in the IIR faculty, as well as for granting the scholarship from which I benefited in the first 3 years of doctoral training.

I thank all colleagues and collaborators at American PAN Europe for their understanding, moral support and applied technical discussions, based on which I was able to design the experimental programs for electrical resistance relief welding. I am glad to have contributed, through the various experiments performed and the procedures developed for the documentation of the resistance relief welding technologies, to the implementation of the optimized technologies at American PAN Europe. I would also like to thank my parents and family for all their support, patience and encouragement throughout my PhD studies. It has been a sustained effort but also an honor to contribute to the scientific progress in the field of relief welding, to write and present research papers at various specialized conferences in the country and abroad.

Bucharest, 2026

Yours sincerely,

Eng. Alexandru Vlăduț OPREA

INTRODUCTION

The doctoral thesis entitled " RESEARCH ON THE BEHAVIOR TO ELECTRIC RESISTANCE WELDING BY PROJECTION OF THIN ALUMINIZED STEEL COMPONENTS" includes the documentation, research and experimentation that have been carried out to study the phenomena occurring in electrical resistance relief welding, in the case of thin aluminized steel sheets. The theme of this PhD thesis was shaped because of the work carried out as an engineer trainee at Pan American Europe in Alexandria, Teleorman, following the observation of some problems regarding the quality of welded products made on the technological flow of manufacturing aluminized steel trays. On this occasion, I analyzed the effect of the welding regime parameters and tested several sets of welded samples, made with different values of these parameters, which allowed me to improve the performance of the manufactured products, reduce costs by reducing energy consumption and minimizing the number of scrap products. Although the topic seems simple, it took several sets of experiments performed with different pairs of welding parameter values to finalize and document the welding technology, and ultimately to implement it in production and thus contribute to the increased profitability of the organization.

Therefore, I consider this work to be valuable, both for my professional training and for the field to which it is addressed. The results that I have obtained from the applied research have been very useful to me and represent an element of progress for the company where I work or for other companies that manufacture welded structures from thin components, being at the same time a model of approach to the topic of resistance welding for industrial engineering specialists.

***

In the first chapter of the PhD thesis entitled "General elements on the state of the art in the field of electric resistance welding" the most important aspects of the electric resistance welding process are briefly presented, starting from the classical spot-welding schemes and ending with the derived relief welding process. The chapter presents the advantages and disadvantages of the electric resistance and pressure welding processes, the effects of the technological process parameter values on the quality of the weld spot and the overall joint strength. Prospects for improvement of the welding process and methods of adjusting the process parameter values to obtain the best results are analyzed. The factors contributing to the correct formation of the weld spot, the influence of the working mode on the welding electrodes, the thermal equilibrium in the weld spot area and their effects on the liquid metal expulsions are analyzed. It also presents the main methods of checking the values of electrical parameters in welding, non-destructive testing of welded spots and quantitative quality assessment by destructive methods. Finally, the most important conclusions drawn from the analysis of the performance and improvement possibilities applicable to the electric resistance welding process in the case of thin steel sheets are presented.

In the second chapter, entitled "Electric resistance welding behavior of thin steel components", the factors influencing the electric resistance welding behavior of steels are analyzed, such as: the effect of the coating layers (which ensure corrosion resistance) on the correct formation of weld spots; the cooling rate during welding; problems occurring in the realization of heterogeneous joints; the welding regime; the mechanism of weld spot formation. At the end of the chapter the important conclusions are summarized.

important ideas derived from the analysis of the current state of the art in the field of electric resistance welding.

The third chapter is entitled "Objectives and structure of the PhD thesis. Research apparatus", having as object the presentation of the stages that allowed the realization of the thesis, the way in which the studies, research and experiments were planned and carried out, as well as the apparatus that was used during the doctoral program in order to achieve the proposed objectives.

The first 3 chapters of the thesis, totaling 38 pages, represent the part of theoretical documentation and planning of the experimental program.

Chapters 4, 5 and 6 are contained in the second part, which includes original research, experimental programs carried out, welding technology, mechanical tests and structural analysis.

In the fourth chapter, entitled "Experimental Investigations of Relief Welding of Thin Aluminized Steel Components" with 24-page extension, the complete program of experiments carried out to study the welding behavior of thin aluminized steel components under pressure relief welding is presented. For this purpose. The base materials used (1.2 mm and 0.8 mm thick sheets coated by aluminizing with a thin Al-Si alloy protective layer) are analyzed. Optical microscopy analyses were performed to evaluate the compactness and appearance of the aluminized layer, as well as SEM and EDAX electron microscopy analyses to evaluate the chemical composition of the aluminized layer, its adhesion and compactness to the steel substrate. Then the samples were prepared for welding by cutting strips of length 150mm, width 45mm and overlap width about 52mm. The 0.8mm thick steel samples were overlapped on the 1.2mm thick samples (on which the protrusions were made by stamping with dedicated punches with 3 or 5 protrusions each) and then welded according to the developed welding technology. After welding the first batches of samples, the imperfections that appeared during welding were evaluated in order to optimize the assembly process. At the end of the chapter, the main conclusions resulting from the analysis of the welded samples are specified.

In the fifth chapter, 36 pages in length and entitled "Characterization and Testing of Welded Specimens by Electrical Resistance Welding in Relief", the detailed analysis of the welded joints carried out in the previous chapter was continued. For this, sampling was carried out by cutting out the welded areas and obtaining cross-sections through the welded points using the precision cutting machine. The samples were then embedded in phenolic resin and subjected to metallographic processing with progressively grained abrasive papers and then with liquids with fine abrasive particles in suspension. For the chemical micro-composition analysis with the EDAX method, the sample surfaces were not etched in order not to contaminate them with elements of the chemical reagent. Microstructural analyses were performed by optical and electron microscopy SEM. This was followed by microhardness measurements on the welded spot micro areas and thermal influence zones to evaluate the effects of the aluminized protective coating on the correct weld spot formation. In the remainder of the chapter, continuous tensile rupture tests were carried out on the welded specimens, the rupture diagrams and mechanical parameter values were recorded, and the specimens were analyzed to identify the mode of rupture. Indices for the prediction of the failure mode were then calculated, and the values were compared with the results obtained by the experiments. The chapter concludes with the main conclusions drawn from the analysis of the experimental and theoretical results.

The sixth chapter, titled "Optimization of the Relief Welding Process" and spread over 44 pages, presents the experimental model for the optimization of the regime parameter values for relief welding of thin aluminized steel components. The optimization method used was proposed by Taguchi. For this purpose, 2 orthogonal matrices were designed, one for welded specimens with 3 protrusions and one for those with 5 protrusions. For the design of the experiment matrix, the factors defining the technological regime of electric resistance welding in relief were determined and were the basis of the optimization process, namely: welding power, Ps (kVA); welding time, ts(ms); electrode pressure, p (bar). The number of parameters that effectively influenced the electric resistance welding process were three (P= 3), each having four optimization levels (L = 4). For the evaluation of the welding process, new sets of 3- and 5-protrusion welded specimens were made with the same values of the regime parameters set on the criteria of high mechanical strength at high tear, medium strain at medium tear and localized tear only in the base material. The samples were tested at continuous rupture and the results obtained were analyzed based on the established optimized behavior criteria. At the end of the chapter, the conclusions of the experimental investigations carried out are presented and appendices are developed presenting the specifications of the welding procedures used to obtain specimens.

Chapter seven, entitled Contributions and Conclusions. Further research directions" summarizes the main contributions of the author in the field of the PhD thesis and the conclusions drawn from the research and experiments carried out.

***

The program of advanced training through doctoral studies carried out within the Doctoral School of FIIR of UPB was conducted under the coordination of Prof. Prof.dr.dr.ing. Ionelia Voiculescu and included the following stages of preparation:

- documentation on the field of the PhD thesis, for which more than 180 bibliographical references published at national or international level were consulted (most of them after 2015).
- preparing and taking the specialized and general preparation examinations as part of the doctoral training program.
- Drafting and presentation of 5 scientific reports (Scientific Report 1 - General elements on the state of knowledge, objectives andmethodology of research - development in the field of resistance welding; Scientific Report 2 - Research on the effects of the parameters of the technological regime on resistance welding; Scientific Report 3 - Research on the behavior of some steels in resistance welding; Scientific Report 4 - Electric resistance welding technology. Program of experiments and tests on welded specimens; Scientific Report 5 - Research on the electrical resistance welding behaviour of thin aluminized steel components).

- design of the electric resistance relief welding technology of thin aluminized steel components which was implemented in *American PAN Europe, Alexandria, Jud. Teleorman*
- realization of the welding technology documentation (SPS/WPS 320 - 327).
- drafting the manuscript for the doctoral thesis, revising it based on the proposals made by the members of the tutoring committee and the doctoral supervisor.
- drafting manuscripts and publishing articles and scientific papers.
- participation in the skills training project entitled "OPTIMizing the results of applied research of doctoral students and postdoctoral researchers" - OPTIM Research, organized by the Romanian National Committee of the World Energy Council (CNR-WEC), Co-organizer of Advanced Applied Research Internships.
- participation in training programs such as: Autodesk Inventor: Essentials (Autodesck Platinum Partner, Man and Machine Education Center, Man and Machine Education Center, Bucuresti), Conversational English - Europass C1, Certificate of Graduation (British Academy of Business and Communication, 27.06.2020), Robot Operation and Programming (TPEB)-FANUC Automation Romania SRL, 06.03.03.2023 - 10.03.2023, Laser Safety Training Course (suitable as training for a Laser Safety Officer) coordinated by Dr. Anna Bass - Lasermet LTD, UK, 20.04.2023, Computer System Programmer - Project co-funded by the European Union, "CoreComp-Competences for Employees", 27.01.2025 -2026.
- Participation in specialized conferences in the country and abroad - Brasov (International Conference Bramat, 16 March 2024), Bucharest (Workshop DIGITAL 4PPP -24 November 2023; Conf. ICMaS, November 16, 2023, Welding Conference, April 3-4, 2025), Cluj-Napoca (April 7-8, 2022), Bosnia (International Congress EEM, March 20-23, 2023).

CONTENTS

Chapter 1. General elements on the state of the art in resistance welding		7
1.1.	General aspects of electric resistance pressure spot welding	7
1.2.	Pressure relief electrical resistance electric resistance welding (SPRER)	9
1.3	Advantages and disadvantages of the SPRER process	10
1.4	Control of process parameters during welding	11
1.5	Destructive and non-destructive spot testing in relief welding	12
Chapter 2. Electrical resistance spot welding behavior of steel sheets		13
2.1.	Factors influencing the resistance welding behavior of steels	13
	2.1.1. Protective layers present on the surfaces of welded components	13
	2.1.2. Welding cooling rate	14
	2.1.3. Welding regime	14
2.2.	Weld spot formation mechanism	15
Chapter 3. Objectives and structure of the thesis. Research apparatus		16
3.1.	Objectives of the doctoral thesis	16
3.2.	Structure of the doctoral thesis	17
3.3.	Research equipment used for the experimental program	18
Experimental part		
Chapter 4. Experimental research on relief welding of steel components		19
4.1.	Experimental investigations on 3-point relief welding of steel components	19
	4.1.1 Materials used	19
	4.1.2 Welding preparation	23
	4.1.3 Preliminary investigations to establish the welding regime by resistance relief welding	23
4.2.	Experimental research on 5-point relief welding of steel components	27
	4.2.1 Materials used	27
	4.2.2 Preparation of samples for welding	28
	4.2.3 Welding of 5-protrusion specimens	28
4.3	Welding imperfections	30
Chapter 5. Characterization and testing of electric resistance welded specimens		33
5.1.	Microscopic analysis	33
	5.1.1. Base material analysis	33
	5.1.2 Analysis of 3-protrusion welded specimens	35
5.2	Burst testing	41
	5.2.1 Tensile test results for 3-protrusion welded specimens	43
	5.2.2 Tensile test results for welded specimens with 5 protrusions	43
5.3	Hardness measurements	44
Chapter 6. Optimization of the relief welding process		45
6.1	General aspects	45
6.2	Performance of the samples according to the optimized experimental program	46
Chapter 7. Conclusions and contributions. Future research directions		48
	Bibliography	50

Chapter 1. STATE OF THE ART IN ELECTRIC RESISTANCE WELDING

1.1 General aspects of electric resistance pressure spot welding

SPREP is a process that utilizes the resistive effect of electric current to spot heat and melt two or more overlapping workpieces clamped with a specified force between contact electrodes. Limited areas of rapid transfer of electric current are formed in the areas of contact between the surfaces of the parts, and the high contact resistance between them causes heating and melting of the area under the welding electrodes. Regardless of the processing method, the metal surfaces of the components are not perfectly flat but have a certain roughness.

The resulting weld spot has a lenticular shape and is in the plane of separation of the components.

In direct electric resistance spot welding, the contact electrodes are placed on opposite sides of the components (fig. 1.1)

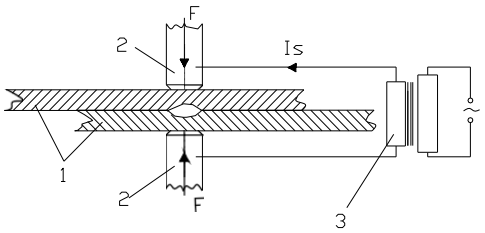


***Fig.1.1**. Principle of direct electric resistance spot pressure welding.*
1. welding components; 2. contact electrodes; 3. voltage source for welding current supply [1].

The contact area between the electrode and the sheet is a very important parameter that contributes to obtaining a proper weld quality in direct correlation with the electrode resistance [16-17]. One can analyze the variations of the contact area by observing the electrode resistance variations. Thus, the lower the resistance, the larger the contact area between the components.

To measure the contact resistance, the test device is connected to the two electrodes, and when the prescribed force is applied without current flow, the change in resistance values is recorded. The amount of heat generated in the weld spot area depends on the thermal conductivity and electrical resistance of the metal, as well as the time of holding current through the joint [19-24]. The heat generated by Joule-Lenz effect can be expressed by the equation:

$$\mathbf{Q} = \int_0^t \boldsymbol{R(t)I^2\,(t)dt} \qquad (1.1)$$

Or by the simplified equation:

$$\mathbf{Q = I^2RtK} \qquad (1.2)$$

where "Q" is heating energy [kJ or J], "I" the welding current [A], "R" the total electrical resistance [Ohm], "t" the time of current application (can be expressed in hertz, milliseconds or microseconds), K is a thermal constant that depends on the geometry of the parts, the clamping mode and the amount of force applied during welding [25]. In addition to Joule heating, other thermoelectric phenomena such as the Peltier effect and the Thomson effect also exist in the resistance welding process.

The contact resistances between the electrodes and the parts, as well as between the overlapping parts for welding, on which the temperature distribution at the welding zone level depends, are: RΩ - ohmic resistance of the base metal, Rpp - contact resistance between the parts to be joined, Rcp - contact resistance between the copper electrodes and the workpiece. From Fig. 1.2 it follows that **RΩ** increases with temperature, while the contact resistances between the weld pieces (**Rpp**) and between the copper electrode and the workpiece, (**Rcp**) decrease rapidly as the temperature of the workpieces increases.

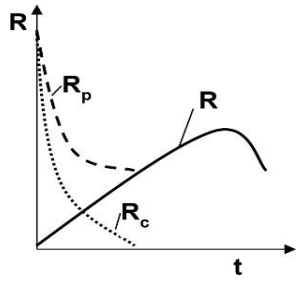


***Fig. 1.2**. Diagram of variation of resistances at resistance spot welding.*

Zwolsman [30] proposed a relation for estimating the value of contact resistance as follows:

$$Rc = \frac{\rho}{2}\sqrt{\frac{\pi Hb(T_1 - T)}{3F(T_1 - T_2)}}\left(\frac{T}{T2}\right)$$

(1.3) where Rc - contact resistance, ρ - electrical resistivity of the material, Hb - Brinell hardness at room temperature, F - pressing force, T - operating temperature (K), T1 - softening temperature (K), T2 room temperature.

The contact resistance found in the general scheme of an electric resistance welding process are shown in Fig. 1.3. The large amount of localized heat over small areas causes the initial bridges to "collapse" and form new peaks of the contact surfaces, i.e. new bridges or additional current paths. Since the resistivity of the molten metal is higher than that of the new solid bridges, the current flow is transferred mainly on these, and the process continues until the entire interface is reached in the liquid state.

R_{c1} - contact resistance between the surface of the upper electrode and the upper part

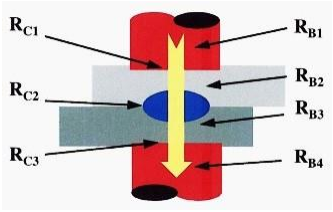
R_{c2} - contact resistance between the two pieces superimposed

R_{c3} - contact resistance between the lower part and the surface of the lower electrode

R_{B1} - electrical resistance of the upper electrode.

R_{B2} - electrical resistance of the upper part; R_{B3} *(Resist)*

- electrical resistance of the lower part; R_{B4} - electrical resistance of the lower electrode.



(Fig.) (1.3.) *Electrical and contact resistance in resistance spot welding [47].*

The next step is to increase the pressing force of the electrodes to forge the molten zone. When the the molten metal solidifies rapidly, forming the weld spot. The total electrical resistance ($_{RT}$) can be expressed by the relation:

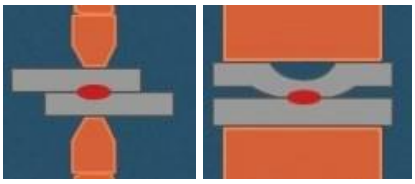
$$_{RT} = \square^{1} + \square_{\square} + \square^{\square\square} \qquad (1.4)$$

Where $\square_{\square}^{1}$ is the contact resistance between the copper electrodes and the surfaces of the parts to be welded, $\square_{\square}^{2}$ is the contact resistance between the surfaces of the parts, and Rp is the volume resistance of the part material through which the electric current is flowing when welding. The value of the term $\square^{2}$ can be influenced by the degree of surface cleanliness, the presence of coatings, roughness, etc. The value of the contact resistance between the surfaces of the workpiece surfaces increases with decreasing roughness [171] rust or other impurities.

1.2. Pressure welding with electrical resistance relief electric resistance (SPRER)

The process of pressure welding with "raised" electrical contact resistance (SPRER) is derived from the general scheme of spot resistance welding (SPREP), except that in this case the joint areas are provided with contact points obtained by local deformation of the surface (indentation) in order to concentrate the current lines during welding (Fig. 1.4). With increasing temperature up to the melting temperature, due to the decreasing mechanical strength of the materials, the protrusions flatten under the influence of the pressing force, and the welding proceeds in a similar way to spot welding. The main difference in projection welding is that flat-surfaced electrodes are used, which are connected to the secondary of the step-down transformer. The joint is formed at distinct points, determined by the existence of protrusions on one of the components. On the surface of the protrusions there is a concentration of electric current and pressing force, which causes them to heat up and deform rapidly.

Obtaining quality joints depends, first and foremost, on the careful design of the protrusions and on ensuring that the surfaces are clean so that the welding current and the pressing forces are distributed as evenly as possible over the protrusions.



a) spots *b) projection*

***Fig. 1.4**. Comparison of the schemes of pressure welding with electrical contact resistance. a) spot: b) projection [6].*

Relief welding is applicable for both thick components and for miscellaneous assemblies between components of small or different thicknesses. To ensure thermal equilibrium, the thicker component is embossed to obtain areas of current concentration when welding. The dimensions of the projections depend on the thickness and the mechanical strength value of the components.

In the case of thicker components, it is more difficult to machine these protrusions and special machining operations are required. Therefore, in some cases, it is preferable to make projections on the thinner component. Protrusions can be made in such a way that several areas of the part can be welded at the same time.
at the same time (Fig. 1.5).

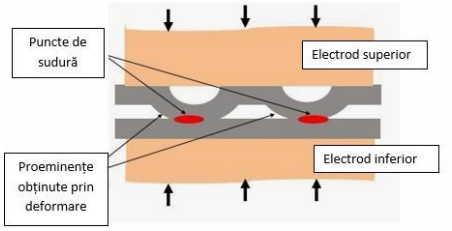


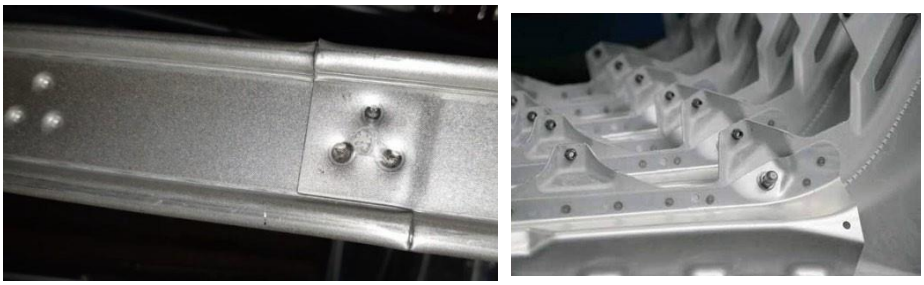
***Fig. 1.5**. Simultaneous formation of several weld spots [8].*

Overall, the electrical resistance relief welding process accounts for 20-25% of all resistance welding applications in manufacturing [17]. Because heating is concentrated at the small cross-sectional protrusions, the welding process requires less energy and time than traditional electric resistance spot welding. The method can be applied using both individual hand-operated machines and automated systems.

1.3. Advantages and disadvantages of the SPRER process

The main advantages of the SPRER process are:

- The quality of the weld is very good, and the productivity of the process is very high, as several welding spots can be made simultaneously (Fig. 1.6);



a) b)

Assemblies made by the SPRER process with several simultaneous spots between sheet metal components. a) aluminized steel; b) aluminum [6].

- Production can be mechanized or automated, assemblies can be made between components with different thicknesses and different geometries; the process has no limitations on component thickness, the positioning of the joining points being the designer's option, depending on the functional role of the assembly.
- In difficult welding conditions the effects of heating of the welded components or the design of metal spatter are reduced, their deformation being minimized.
- The total electricity consumption required for welding is lower compared to the SPREP process, which brings economic advantages after the implementation of welding systems.

The following can be listed as disadvantages:

- Not all torques of material types can be welded with this process, thickness or chemical composition can be sometimes a problem.
- Materials that do not provide sufficiently good mechanical strength of the protrusions cannot be deburred under optimal conditions. For example, some copper alloys or copper alloys cannot be welded satisfactorily with this process.
- An additional machining process of one of the components is necessary to obtain protrusions of sufficient size to be able to make the welding spots (additional production costs and operating time);
- The contact point of the protrusion must be at least equal to the smallest thickness of the metal being welded.
- Sometimes the appearance of welded spots is unsightly, welded areas can be considered Unitary stress concentrators or corrosion localization.
- Welding electrodes have a large contact surface, and layers can be deposited layers can be deposited from the welded parts, requiring periodic cleaning.

1.4 Control of process parameters during welding

In electric resistance spot pressure welding applications, there are a number of methods used to monitor, control and react to normal variations in process, material and equipment program conditions. The actual welding time may be longer (10 ms) than the protrusion deformation time (5-6 ms). During this time, the welding equipment must "monitor" the protrusion height value (0.5 - 1.0 mm) while maintaining the welding pressure force value. Consequently, the main difficulty is the ability of the welding regime parameter value control system to continuously adapt to changes in electrical resistance, plastic deformation level and pressing force value to achieve a weld of the required quality [4].

The pressing force should be kept constant throughout the welding process but can be increased slightly in the latter part of the process to provide an additional forging effect. Depending on the size and type of material being welded, the welding time can vary from a few milliseconds to 1 second (i.e. 50/60 cycles) (Fig. 1.7).

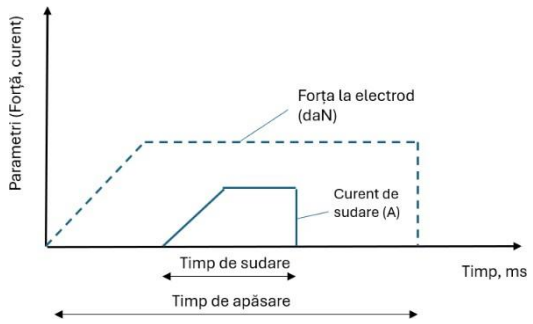


Fig. 1.7*. Evolution of the regime parameters for welding*
welding.

The total energy (Energy= Power x Time) can be the same for a welding process placed in quadrant II and IV, but the speed of energy delivery is essential for relief welding. The size of the process window can be increased by proper selection of materials (electrodes and workpieces), designing the shape of the workpiece protrusions, choice of welding equipment and welding process parameter values. A wider process window allows a robust process that is not sensitive to normal part variations. As the number of impressions (bosses) increases, the current and pressure on a boss decrease. The protrusions do not weld simultaneously, and the pressure and current distribution is not uniform. For example, for a 1 mm thick steel sheet, the following parameter values occur: for a protrusion the welding current= 8000 A and the pressure on a protrusion is 480 kg, for 5 protrusions the welding current is 4600 A and the pressure on a protrusion 400 kg. When welding aluminum relief, protrusions deform very easily during welding. For this reason, pneumatic cylinders must be fitted with a resilient element, placed between the cylinder and the electrode, to compensate for the collapse of the protrusions. The distance between protrusions must be at least three times their diameter. When relief welding components of different thicknesses, an electrode of lower electrical conductivity should be placed on the area of the thinner component [40-42].

To assess the degree of surface preparation, the contact resistance can be

measured on small specimens using special installations placed outside the welding machine (Fig. 1.8).



***Fig. 1.8**. Apparatus for measuring electrical resistance values in relief welding [25].*

1.5 Non-destructive and destructive testing of spots in projection welding

Non-destructive examination can be applied for welded raised spots using the ultrasonic method. The ultrasonic pulse passes completely through the welded core between the two welded parts and is received by the transducer. In this way the integrity and continuity of the weld area is checked. If there is a defect, the reflected wave will be asymmetric, with reflection at a depth or distance different from the normal value (Fig. 1.9). Resistance spot welding is the most important joining process used in the mass production of car bodies, which is why it is necessary to ensure a high-quality level of the welded spots [39].



***Fig. 1.9**. Ultrasonic non-destructive examination of weld spots [26].*

The temperature distribution can be calculated from the electro-thermal analysis for a given time interval, then a thermal load value is imposed on the thermomechanical analysis module [45, 46]. This procedure is repeated, a certain time interval (called the refresh rate), until the entire welding cycle is fully completed (Fig. 1.11).

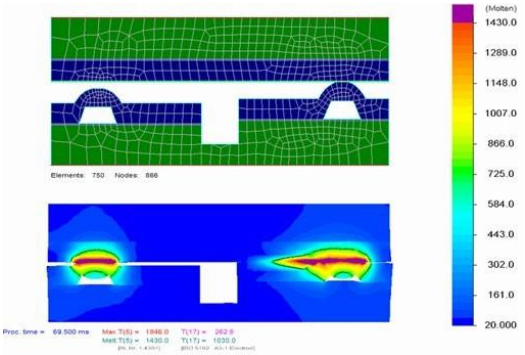


***Fig. 1.11**. Finite element diagram of the relief welding process [28-29].*

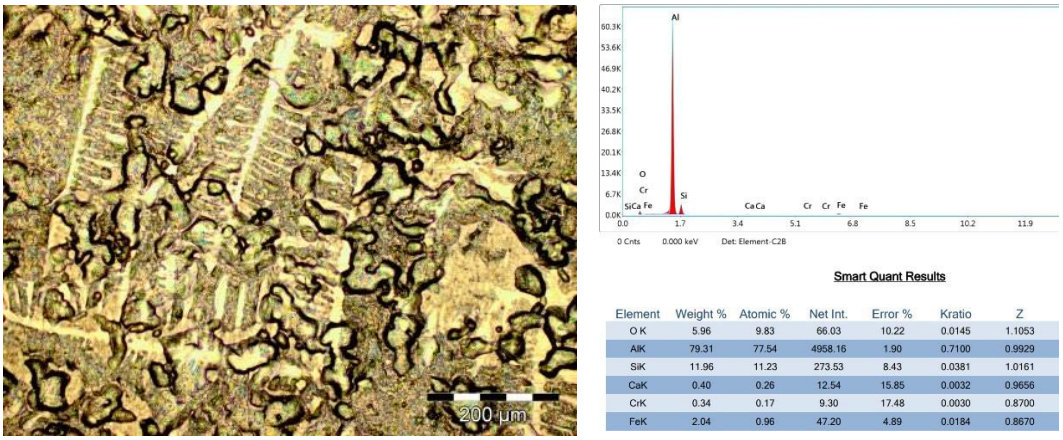
Chapter 2 WELDING BEHAVIOR DURING OF THIN STEEL COMPONENTS

2.1 Factors influencing the resistance welding behavior of steels

Thin steel components are often joined with the electric resistance spot welding process because the large difference in electrical resistivity compared to electrodes made of copper allows an optimal localization of the melt zone at the interface between the parts.

2.1.1 Protective layers present on the surfaces of welded components

The appearance of the aluminized surface depends on the coating process, the thickness of the deposit, the chemical composition of the deposited material and the nature of the substrate (Fig. 2.1.). Aluminized steel is now widely used in the manufacture of baking pans. The thin layer of food-grade aluminum improves corrosion resistance and facilitates the extraction of products from the baking pans. According to the EDS analysis performed on the surface of the aluminized steel sheet, the chemical composition contains (% by weight): 79.31% Al; 11.96%Si; 2.04 Fe; 0.34%Cr; 0.40%Ca; 5.96%O [62-64].



a) b)

Fig. 2.1*. Aluminized layer aspect (a) and EDS analysis on the coating surface (b) [36, 64].*

2.1.2 Welding cooling rate

One of the main problems arising when welding high-strength steels is the formation of martensite in the heated zones above the temperatures corresponding to the transformation point temperatures because of rapid cooling. For component thicknesses up to 2 mm, the weld spot usually solidifies in less than three to four current cycles. By modeling, it has been shown that even at 500°C, cooling rates in spot welding exceeded 1000°C/s [79]. For steel, the critical cooling rate (v) required to obtain martensite in the microstructure is given by Eq:

log v = 7.42 - 3.13 C - 0.71 Mn - 0.37 Ni - 0.34 Cr - 0.45 Mo (2.1)

2.1.3 Welding regime

Frequent problems in resistance welding are related to the expulsion of molten metal between the components in the forging stage, i.e. the formation of spatter or buildup at the edge of the weld spot. This phenomenon occurs at excessive values of pressing forces, at too high values of welding current and welding time, when the surfaces are not properly aligned or there is too much play between them, which allows liquid metal to leak out [62-64]. Increasing ***the welding time*** value causes the molten core size to increase. As the current increases, the heat generated in the weld spot volume will be greater, but at the same time, the increase in electrode pressure causes the contact resistance to decrease, which results in a decrease in the amount of heat generated by the Joule effect and consequently a smaller weld spot volume [76].

Weld spot size has often been a measure of joint quality, but results from studies have shown that appropriate weld spot breaking strength values can be obtained even with small-diameter, multi-point welds in low-carbon steels. Additional tests, such as fatigue or impact tests, have confirmed the applicability of multi-point joints [52]. Usual values for the average diameter of the weld spot are established as a function of component thickness with the relation:

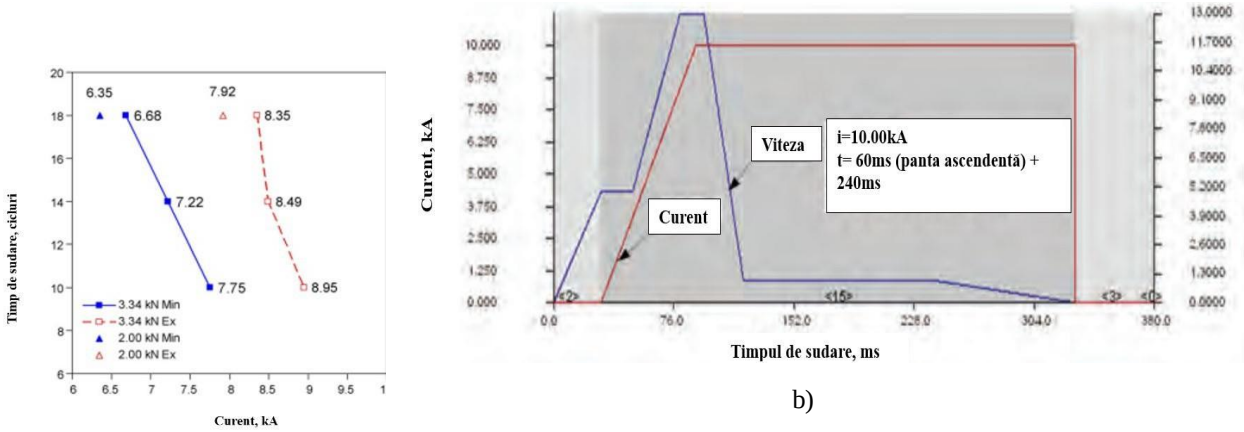
$$\mathbf{D = 4\sqrt{t}} \text{ or } \mathbf{D\ 5\sqrt{t}=} \qquad (2.2)$$

where t is the material thickness in mm [85]. In steels, the best results were obtained for values of D = 2.7t + 1.6 [94, 125].

Electrical contact resistance is a key factor in the electric resistance welding process [86]. At the microscopic scale, interface phenomena depend on the contact between surfaces, which is often imperfect because there are different roughness, oxides or other dielectric media that generate a micro-constriction effect of the electric current lines, which influences the amount of heat that is generated in the micro volumes of material [87-89]. The state of the contact surface introduces uncertainty in welding, making it difficult to directly measure the dynamic resistance in the type of weld spot formation. Model design of the real workpiece using an artificial neural network has demonstrated that the input impedance can be used as a monitoring element of weld quality by spot resistance. However, the physical significance of input impedance changes during a welding process is unclear and the calculation of input impedance steps is complex and difficult to understand [90-91].

The pressing force applied to the electrode, current intensity and time are the most important parameters in resistance welding. The desired diameter of the molten core depends on the correct adjustment of the welding current in relation to time. When the time is short, the core diameter decreases, and when the time is long the amount of molten metal increases and the molten metal is projected out of the working zone, with the consequence of decreasing the joint strength [91- 92]. To maintain uniform heating conditions, the electrode pressing force should be gradually increased. When the force is higher, there is a general decrease in the electrical resistance between the two electrodes, which results in an increase in the welding current. Higher values of clamping force result in a larger spot width and fewer voids in the fusion zone.

The amount of welding current is controlled by the current transformer switch, which determines the maximum amount of welding current available. Fig. 2.4a shows the effect of welding current and welding time on the initiation of metal droplet ejections from the molten zone for two values of the pressing forces applied to the electrodes. The electrode travel speed is chosen according to the required force and the mechanical strength of the welded materials (Fig. 2.2b).



b)

Fig. 2.2*. Current-time dependence for resistance spot welding (a) [93] [93] and projection welding (b) [98].*

The value of the peak current Ip is reached in a few milliseconds, during the so-called rise time, tp. The welding time th is maintained until the peak current decreases by 50%, and the total welding time, tl, is maintained until the current decreases to 95% of the peak value [100]. According to the heat field model proposed by Rosenthal, the distribution of temperatures generated by an instantaneous moving heat source can be represented by a point at the molten surface (3-D heat conduction), a line (2-D heat conduction), or a plane (1-D surface heat distribution) that traverses the entire thickness of the components, as in Eq:

$$\boldsymbol{T = To + \frac{\left(\frac{Q}{d^{dim}}\right)}{\rho C(4\pi at)^{\frac{dim}{2}}} \exp\left\{-\left(\frac{r}{2a^{\frac{1}{2}}t^{\frac{1}{2}}}\right)2\right\}} \qquad \textbf{(2.3)}$$

where Q is the power of the heat source (directly related to the welding current, I), d is the material thickness in mm, ρC is the volumetric specific heat, r is the distance from the heat source where the temperature T is determined, T0 is the initial material temperature, t is the welding time, "dim" is the number of dimensions (1 to 3) associated with the heat source selected.

2.2. Weld spot formation mechanism

When projection welding, the dimensions of the protrusions are chosen according to the thickness of the thinner component, the type of materials and the required amount of weld strength. The protrusions can be made with calibrated punches by choosing an appropriate shape of their tip, depending on the material.

Chapter 3 OBJECTIVES AND STRUCTURE THE THESIS. RESEARCH EQUIPMENT

3.1 Objectives of the doctoral thesis

The experimental research aimed to design and obtained sets of relief welded joints, utilizing the knowledge gained from documentation and production experimentation, which allowed to achieve the following objectives:

- Determination of the electrical resistance relief welding regime in joints with 3 or 5 simultaneous welded protrusions, made between sheet steel components with silicon aluminum coating layers.
- Design and production of batches of electric resistance welded specimens
- Characterization and testing of welded specimens using destructive or non-destructive methods.
- Publication of articles and participation in scientific events (conferences, congresses, scientific seminars) in the field of industrial engineering.
- Accumulating technical knowledge and acquiring skills in the design of welding regimes, preparation of technical documentation and interpretation of results, by carrying out experimental and testing programs in specialized laboratories.

3.2 PhD thesis structure

The PhD thesis contains two main parts, a theoretical part including chapters 1, 2 and 3, and an experimental part including chapters 4, 5 and 6 (Fig. 3.1).

To these main chapters are added the bibliography, the appendices containing the technological documentation for the realization by relief welding of sheet steel components, the presentation of the author's scientific career and the introduction pages.

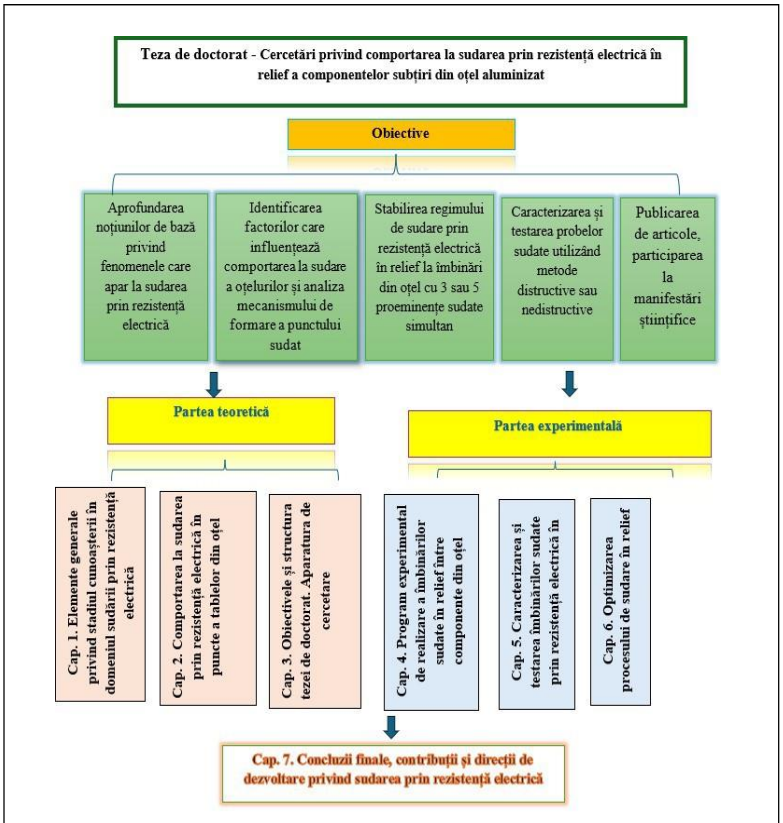
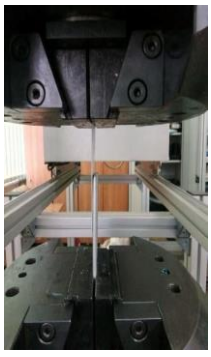


Fig. 3.1 Reprezentarea schematică a structurii tezei de doctorat

3.3 Research apparatus

Several apparatuses were used for the realization of the objectives proposed in the thesis, machines and industrial equipment, which are summarized in Table 3.1.

Table 3.1. Research apparatus used to carry out experiments

Name of apparatus, technical data	Name of apparatus, technical data
TECNA 8005D Series TECNA 8005D Electric Projection Resistance Welding Machine (maximum welding power 200 kVA, maximum welding current for steel 28 kVA) 	Hydraulic dynamometer for electrode force measurement. Measuring range: maximum 1600 daN. Recommended range of use: 200-1400 daN. Required electrode stroke: minimum 20 mm 
Portable device for measuring electrical and time parameters in resistance welding 20 AMADA WELD TECH MM-315B AMADA WELD TECH MM-315B, equipped with portable, multifunctional monitor, measures welding current (kA), welding time/cycles (sec), electrical conduction level (deg), power (%).	
Tensile/compression testing machine "W+b" Walter + bai ag, Switzerland, SIM Laboratory, UPB  	Precision cutting machine for metallographic samples IsoMet 4000. UPB Laboratory. 

SimpliMet 3000 metallographic hot embedding machine. UPB Laboratory. 	Polishing machine for metallographic samples, EcoMet 250 Pro. UPB Laboratory. 
Ultrasonic cleaning system UCI 50, LAMET Laboratory, UPB 	Microhardness Shimadzu HMV 2TE, Japan Measuring range: 98.07, 245.2, 490.3, 980.7mN, 1.96, 2.942, 4.903, 9.807, 19.61N. 
Scanning Electron Microscope, Inspect S, FEI, The Netherlands Laboraor LAMET,UPB.Equipped with EDS chemical composition analyzer, AMRTEC type Z2e  	Inverted optical metallographic microscope, OLYMPUS GX51, Japan, equipped with AnalySIS image processing software 
Digital multimeter, High Resolution Milliohm Meter, resolution below 0.01m 	 Nabertherm LT 15/12/P320 heat treatment furnace

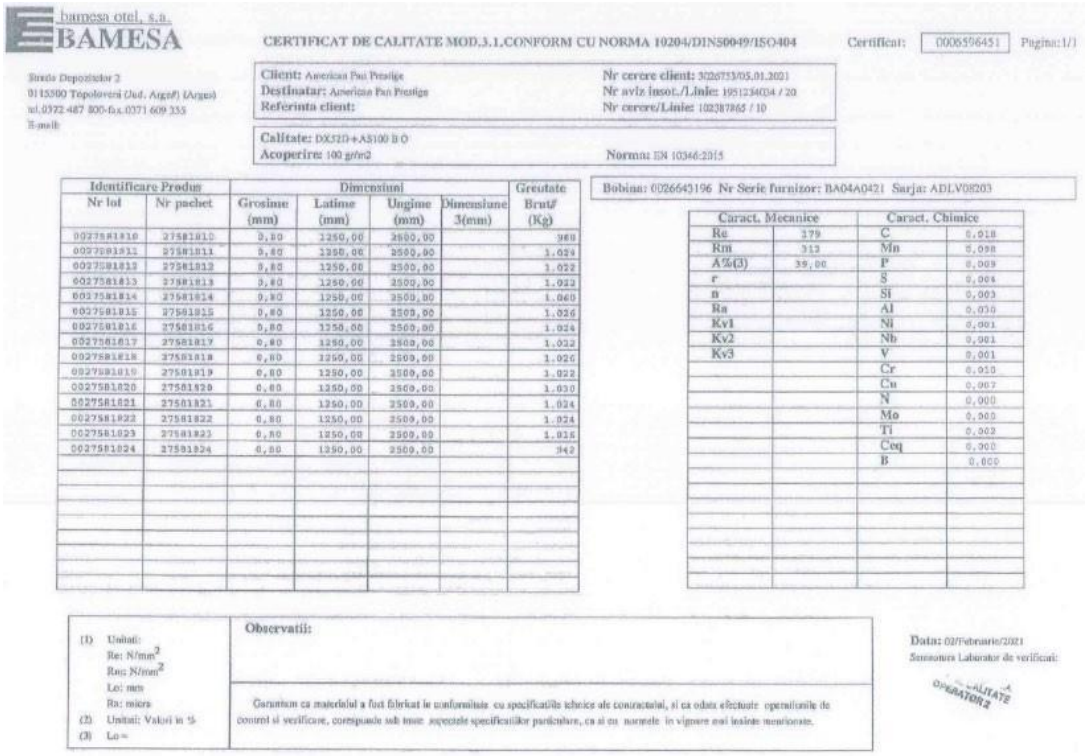
Chapter 4 EXPERIMENTAL INVESTIGATIONS OF RELIEF WELDING OF THIN ALUMINIZED STEEL COMPONENTS

4.1. Experimental investigations of 3-protrusion electrical resistance relief welding of thin aluminized steel components

This chapter analyzes the effect of process parameters on the interface obtained using the projection (relief) electric resistance welding process. The geometry of the welded areas using different values of the welding parameters is analyzed in detail, with an emphasis on the concentration of chemical elements and associated phenomena due to intermetallic compounds occurring at the weld interface. Destructive mechanical tests were used to evaluate the effect of process parameters on the strength characteristics of aluminized steel joints welded in relief.

4.1.1. Materials used

The metal parts that were the subject of the experimental investigations were manufactured from low carbon, deformable, rolled and aluminized sheet steel (trademark DX 52D according to EN 10154: 2002), with thicknesses of 0.8 and 1.2 mm. According to the material quality certificate (fig. 4.1), the steel contains elements such as Al, Cr, Cu, Mn, Si, Ti, Ti, Ni, Nb, V, N, C in individual amounts below 0.01%.



bamesa otel, s.a.
BAMESA

CERTIFICAT DE CALITATE MOD.3.1.CONFORM CU NORMA 10204/DIN50049/ISO404

Certificat: 0006596451 Pagina:1/1

Strada Depozitelor 2
0115300 Topoloveni (Jud. Argeș) (Argeș)
tel.0372 487 800-fax.0371 609 355
E-mail:

Client: American Pan Prestige
Destinatar: American Pan Prestige
Referinta client:

Nr cerere client: 3026753/05.01.2021
Nr aviz insot./Linie: 1951234034 / 20
Nr cerere/Linie: 102387865 / 10

Calitate: DX52D+AS100 B O
Acoperire: 100 g/m2

Norma: EN 10346:2015

Bobina: 0026645196 Nr Serie furnizor: BA04A0421 Sarja: ADLV08203

Identificare Produs		Dimensiuni				Greutate
Nr lot	Nr pachet	Grosime (mm)	Latime (mm)	Ungime (mm)	Dimensiune 3(mm)	Brut/ (Kg)
0027581810	27581810	0,80	1250,00	2500,00		368
0027581811	27581811	0,80	1250,00	2500,00		1.024
0027581812	27581812	0,80	1250,00	2500,00		1.022
0027581813	27581813	0,80	1250,00	2500,00		1.022
0027581814	27581814	0,80	1250,00	2500,00		1.020
0027581815	27581815	0,80	1250,00	2500,00		1.026
0027581816	27581816	0,80	1250,00	2500,00		1.024
0027581817	27581817	0,80	1250,00	2500,00		1.022
0027581818	27581818	0,80	1250,00	2500,00		1.026
0027581819	27581819	0,80	1250,00	2500,00		1.022
0027581820	27581820	0,80	1250,00	2500,00		1.030
0027581821	27581821	0,80	1250,00	2500,00		1.024
0027581822	27581822	0,80	1250,00	2500,00		1.024
0027581823	27581823	0,80	1250,00	2500,00		1.026
0027581824	27581824	0,80	1250,00	2500,00		342

Caract. Mecanice		Caract. Chimice	
Re	379	C	0,018
Rm	313	Mn	0,098
A%(3)	39,00	P	0,009
r		S	0,006
n		Si	0,003
Ra		Al	0,030
Kv1		Ni	0,001
Kv2		Nb	0,001
Kv3		V	0,001
		Cr	0,010
		Cu	0,007
		N	0,000
		Mo	0,000
		Ti	0,002
		Ceq	0,000
		B	0,000

(1) Unitati:
Re: N/mm2
Rm: N/mm2
Lo: mm
Ra: micro
(2) Unitati: Valori in %
(3) Lo =

Observatii:

Garantam ca materialul a fost fabricat in conformitate cu specificatiile tehnice ale contractului, si ca odata efectuate operatiunile de control si verificare, corespunde sub toate aspectele specificatiilor particulare, ca si cu normele in vigoare mai inainte mentionate.

Data: 02/Februarie/2021
Semnatura Laborator de verificari:

Fig. 4.1 *Quality certificate of the basic material - rolled and aluminized non-alloy steel.*

Accompanying elements (S, P) had very low concentrations (S below 0.004% and P below 0.009%). Judging from the low values of alloying elements and carbon equivalent (relation 4.1), respectively, the steel can be considered to have excellent melt weldability.

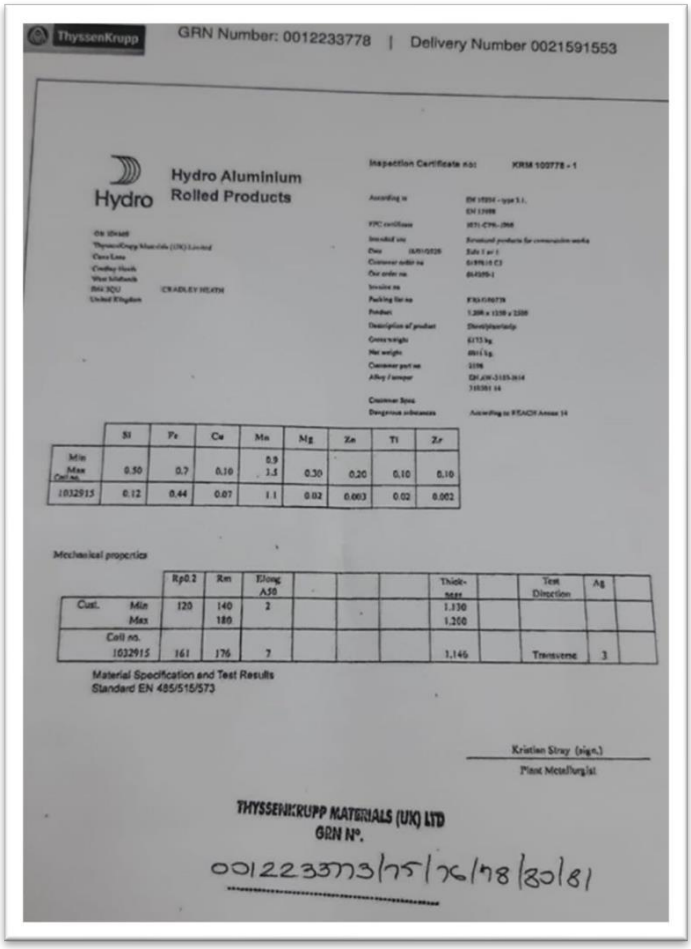
$$Ce = C + \frac{Mn}{6} + \frac{Cr + Mo + V}{5} + \frac{Ni + Cu}{15} = 0{,}037[\%] \qquad (4.1)$$

Ce= 0,018 + 0,098/6+ (0,01+0,001)/5 + (0,007+ 0,001)/7 = 0,037

The critical cooling rate (v) required to obtain martensite in the microstructure (Chap. 2, Eq. 2.1) is:

$$\log v = 7{,}42 - 3{,}13\,C - 0{,}71\,Mn - 0{,}37\,Ni - 0{,}34\,Cr - 0{,}45\,Mo = 1{,}986\ ^{o}C/sec \qquad (4.2)$$

This value is quite low, which means that there are no conditions for martensite. The surface layer deposited by aluminization contains some elements such as Si (0.5%), Fe (0.7%), Ti (0.1%), Mn (0.9 -1.5%), Zn (0.2%), Zr (0.1%), Mg (0.3%), as shown in
chemical analysis certificate provided by ThyssenKrupp (fig. 4.2).


ThyssenKrupp

GRN Number: 0012233778 | Delivery Number 0021591553

Hydro Aluminium Rolled Products

Inspection Certificate no: KRM 100778 - 1

CRADLEY HEATH

	Si	Fe	Cu	Mn	Mg	Zn	Ti	Zr
Min				0.9				
Max	0.50	0.7	0.10	1.5	0.30	0.20	0.10	0.10
Cast no. 1032915	0.12	0.44	0.07	1.1	0.02	0.003	0.02	0.002

Mechanical properties

		Rp0.2	Rm	Elong A50				Thick-ness		Test Direction	Ag	
Cust.	Min	120	140	2				1.130				
	Max		180					1.200				
Cast no. 1032915		161	176	7				1.146		Transverse	3	

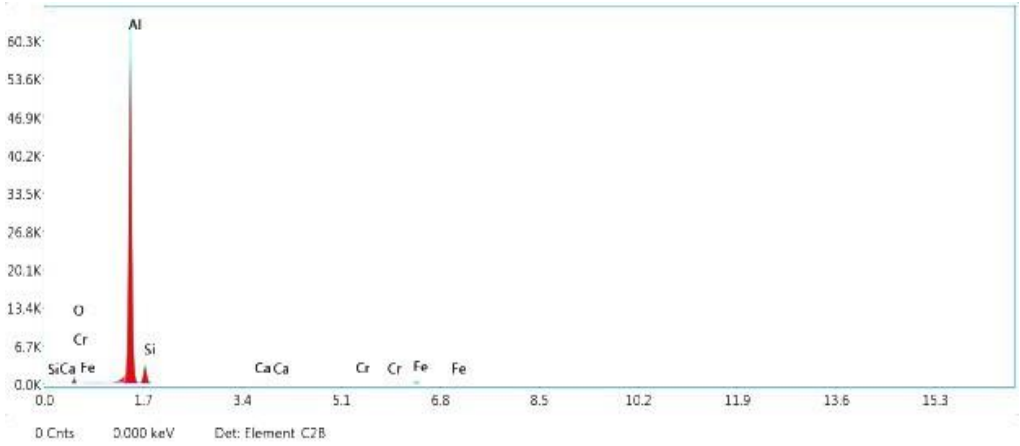
Material Specification and Test Results
Standard EN 485/515/573

Kristian Stray (sign.)
Plant Metallurgist

THYSSENKRUPP MATERIALS (UK) LTD
GRN N°.
0012233778/75/76/78/80/81

Fig. 4.2 *Quality certificate of the coating deposited with food grade aluminum on the steel sheet.*

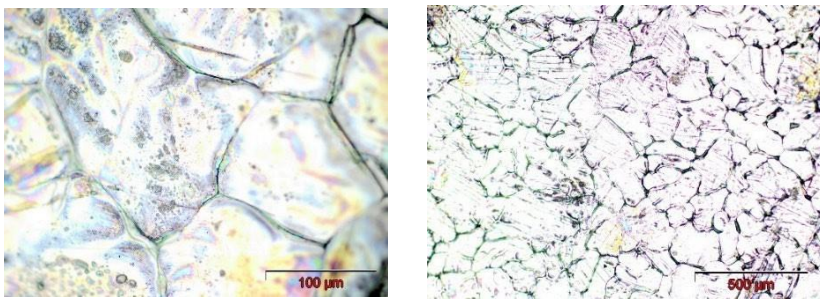
EDAX analysis, using the Inspect S scanning electron microscope equipped with the AMETEC Z2e sensor, showed the presence of the main elements in the aluminized layer, including oxygen (present as aluminum oxide) (Fig. 4.3). According to the EDS analysis carried out on the surface of the aluminized steel sheet, the chemical composition contains (% by weight): 79.31% Al; 11.96%Si; 2.04 Fe; 0.34%Cr; 0.40%Ca; 5.96%O. Chemical composition according to product standard for DX52D steel (1.0350, EN 10154: 2002 Eng. Continuously hot-dip aluminum-silicon (AS) coated steel strip and sheet) is (according to Eng. Technical delivery conditions, EN 10346-2009): C=max. 0,12%; Si=max. 0,5%; Mn=max. 0,6%;
P=max. 0.1%; S=max. 0.045%; Ti=max. 0.3% [17]. Mechanical properties of the material are: yield strength Rm= 270-420 MPa, yield strength $Rp0_{.2}$= 140 - 300 MPa, elongation at break $_{A50}$= 26%. Although the aluminized surface is rougher and more irregular than the Zr- coated surface (Fig. 4.4), the thin layer of food-grade aluminum improves corrosion resistance and facilitates the extraction of products from the baking forms. During welding, the aluminized coating may undergo various changes in thickness, vaporization or expulsion effects from surfaces, and the formation of cracks or agglomerations at the edges of welded spots [35] (Fig. 4.5).



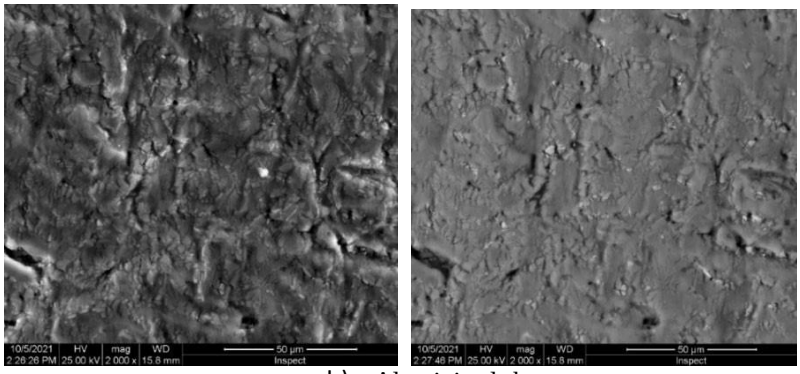
Smart Quant Results

Element	Weight %	Atomic %	Net Int.	Error %	Kratio	Z	A	F
O K	5.96	9.83	66.03	10.22	0.0145	1.1053	0.2195	1.0000
AlK	79.31	77.54	4958.16	1.90	0.7100	0.9929	0.9003	1.0016
SiK	11.96	11.23	273.53	8.43	0.0381	1.0161	0.3137	1.0005
CaK	0.40	0.26	12.54	15.85	0.0032	0.9656	0.8294	1.0129
CrK	0.34	0.17	9.30	17.48	0.0030	0.8700	0.9601	1.0497
FeK	2.04	0.96	47.20	4.89	0.0184	0.8670	0.9848	1.0591

Fig. 4.3 *ADS analysis of local chemical micro-composition on the surface of aluminized steel sheet.*



a) Galvanized sheet



b) Aluminized sheet

Fig. 4.4 *SEM electron microscopy images of the surface of aluminized steel.*
a) galvanized sheet; b) aluminized sheet. LAMET laboratory.

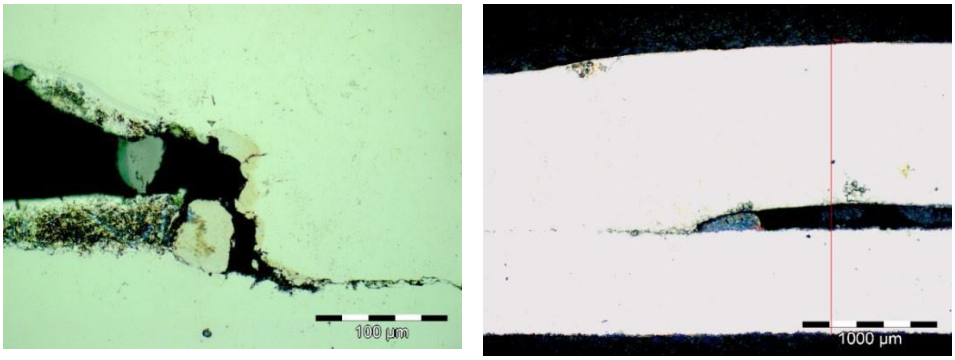


Fig. 4.5 *Compound agglomeration and expulsion-type defects at the edges of welded spots, cracks or lack of adhesion in relief welding of aluminized steel sheets. LAMET laboratory.*

For this reason, in case of aluminized parts it is necessary to perform a larger set of welded samples and tests to validate the welding technology and to choose the optimal values of welding parameters compared to unwelded ones. Optical analysis of the microstructure of the aluminized steel surface microstructure indicates dendritic formations of alpha-aluminum and interdendritic compounds consisting of alloying elements (Fig. 4.6). The parts that were produced in the experimental program were cut from aluminized steel sheet with thicknesses ranging from 0.8 to 1.2 mm, having widths of 32 mm and lengths of 150 mm.

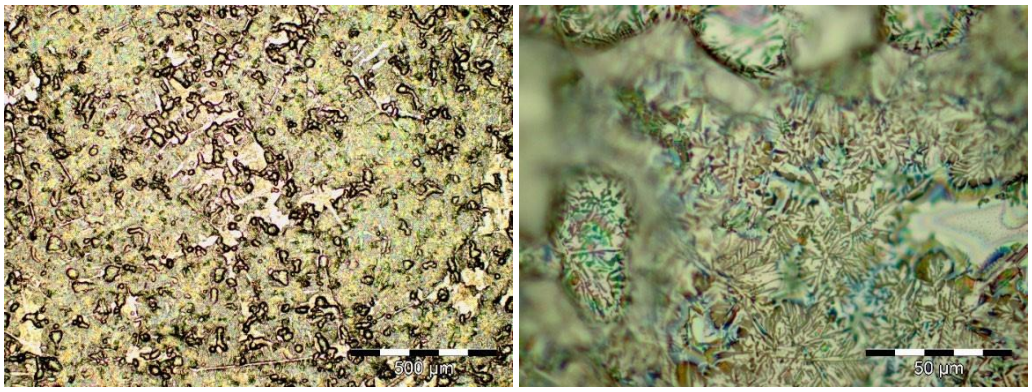


Fig. 4.6 *Surface appearance of aluminized sheets. Optical microscopy. LAMET laboratory.*

4.1.2 Preparation for welding

For the first set of experiments, three protrusions (1.56 mm height and 5 mm base diameter) were made simultaneously on 1.2 mm thick boards, arranged at equidistant distances of 10±0.1 mm, using a 3-pin punching and a tool steel die (Fig. 4.7).

A semi-spherical footprint configuration was chosen to ensure good deformation conditions and to minimize the effects of stress concentrators. The indentations were printed using a 2000 kN shop floor pneumatic press (WC67Y, Shanghai, China) in approximately 1.5 -1.6 seconds per operation (Fig. 4.8).

The sample surfaces were then cleaned with ethanol and dried to avoid contamination before welding.

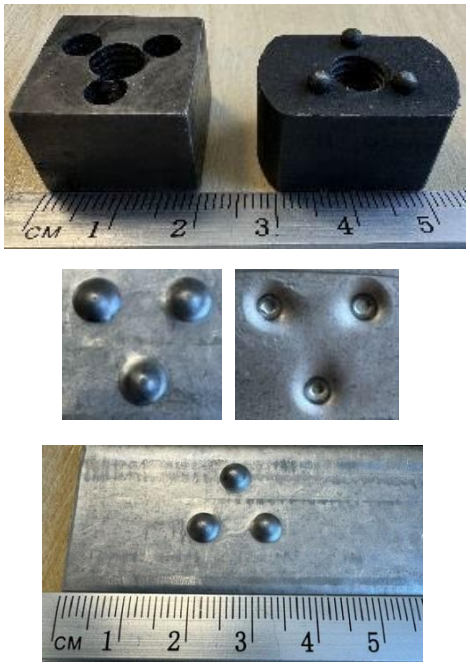


Fig. 4.7 *The die and punch used to execute the protrusions, and the appearance of the protrusions imprinted on the surface of the sheet (front and back).*

4.1.3 Preliminary investigations to establish the relief resistance welding regime

The design of the thermal regime took into account the effects of the main parameters on the melting and solidification of the weld spot. Welding current has a major influence on tensile and shear strength, while welding time and electrode diameter have secondary effects. Joint strength and weld spot area enlargement increase with increasing welding current up to the maximum value [142]. The increase in the hardness value of the joint area is caused by the formation of compounds or hard phases as a result of concentrated heat input and rapid cooling after welding [143].

A TECNA Series 8005D (Ohio, USA) electric resistance welder (maximum welding power 200 kVA, maximum welding current for steel 28 kVA) was used for welding. For the experimental program, RWMA Class III flat-faced copper flat-faced pair electrodes of 99.995% purity, with a working area of 25x25 mm, were used (Chap. 3, Table 3.1).

The Tecna 8005D electric resistance and pressure welding machine is a single-phase AC machine. It has power supply systems and automation possibilities and can be integrated in a robotized cell to increase productivity and high reproducibility of welding processes. The machine is equipped with manual or automatic control systems, which allow both manual and mechanized or robotized operations, with accessories and single-phase welding systems for three-phase direct current and inverter welding sources.

The experimental program used pairs of electrodes made of copper, flat-faced, with a 25x25 mm working surface (Fig. 4.9) or 25 mm diameter.

The length of each sample was 150mm and the overlap length for welding was 52mm. These length values were chosen to be able to carry out the tensile break test later. In the first set of projection welded specimens, a sheet metal blank with a wall thickness of 0.8±0.1mm was used, which was assembled with sheet metal having a thickness of 1.2±0.1mm. On the thicker-walled sheets, three protrusions were made at relatively equal spacings of approximately 10 mm to provide three-point contact with the stiffening strip. The protrusions were welded using the regime parameter values established by the tests (Fig. 4.8). In the first set of experiments, a number of 3 welded points were made simultaneously to obtain a good contact between the two surfaces of the welded parts (Fig. 4.9).



Fig. 4.8 *Electrodes for relief welding.*

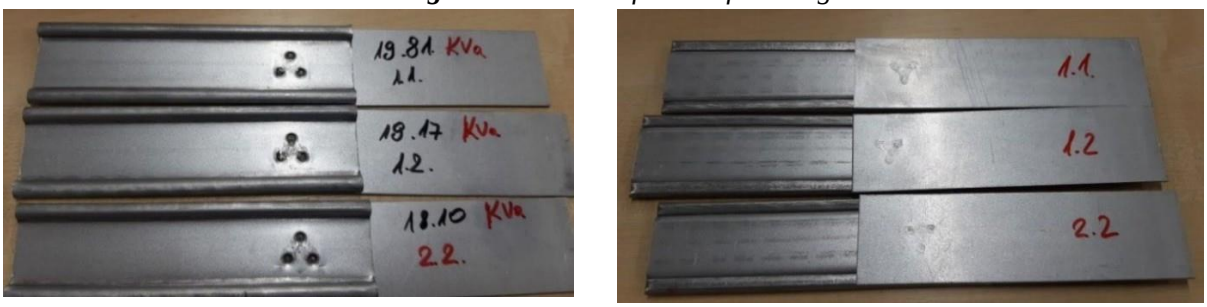




Fig. 4.9 *Welded specimen sets using the electrical resistance relief process (front/side).*

The tables were overlapped by 52 mm in length to limit the effects of molten metal splashing that occur when forging the weld spot. The minimum overlay length for soft regimes is determined by the relation:

$$L_{sup} = 1 + 14{,}4\sqrt{\square} \qquad (4.3)$$

Where t is the thickness of the thinnest component. According to this relationship, the overlap length should have been a minimum of 16.77mm for making a single weld spot. For 3 evenly spaced spots (10mm spacing between adjacent spots), the overlap length should be at least 33.54mm (Fig. 4.10). The length adopted therefore provides the best conditions for spot formation.



Component pressing *Welding itself*

Fig. 4.10 *Sequence of the electrical resistance relief welding of 3 protrusions using 2 pairs of electrodes simultaneously.*

The values of the welding regime parameters are given in Table 4.1. The three main factors of the projection welding regime have been studied: pressing force, electric power and welding time. The pressing force should be set to realize only a small deformation at the tip of the projection before the current passes through the joint. The pressing force may be held constant throughout the welding process or may be increased slightly, in the latter part of the process, to give a forging effect. For low values of the parameters welding force and welding time, the shear strength of the welds decreased. Choosing high values of power and holding time

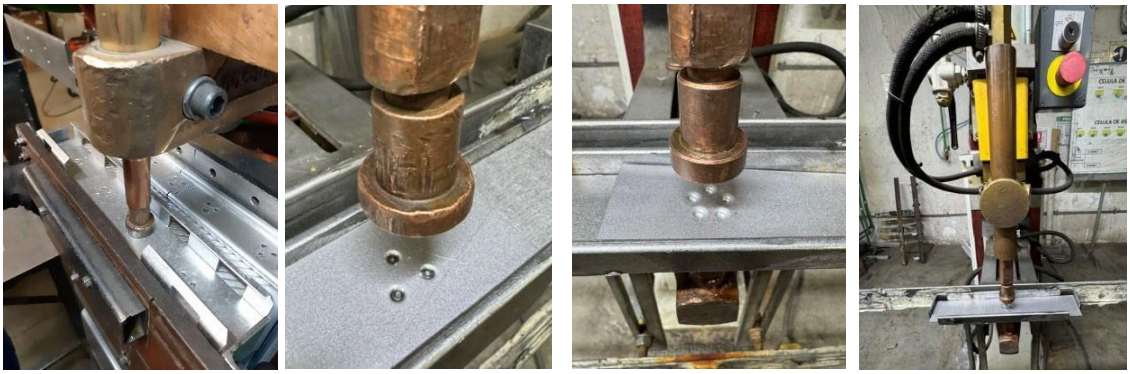
during welding leads to excessive heating and melting of the material, which can cause excessive deformation or perforation of the sample wall [28, 43, 130].

In order to study the effect of the welding regime parameter values, welded specimens with different values of the welding regime parameters were made, which are presented in Table 4.1. The pressing time was kept at the same value for all 3 sets of welded specimens (10 ms), while the welding time was changed from 5 to 7 seconds. The pressure with which the electrodes were pressed on the 2 plates increased from 2.6 to 2.8 and 3.4 bar, respectively. The value of welding power increased progressively from the minimum value of 18.10 kVA to 19.18 kVA and then to 19.81 kVA.

Table 4.1. Parameter values of the welding regime in relief (batches 1 and 2)

Sample	SET	Electrode pressure, bar	Pressing time, ms	Welding time, ms	Welding power, kVA
1.1	1	2,8	10	7	19,81
1.2	1	2,6	10	7	19,18
2.2	1	3,4	10	5	18,10
1.1	2	2,8	10	7	18,08
2.2	2	2,8	10	5	19,57

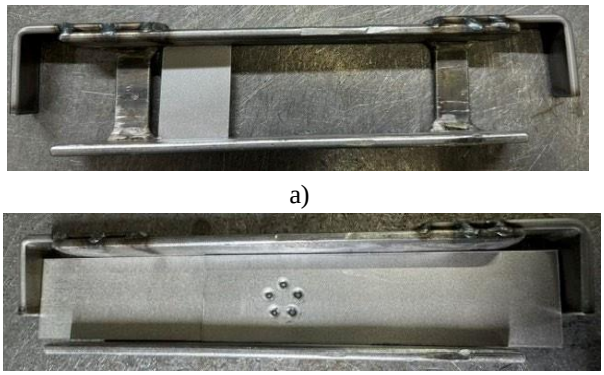
After the first sets of samples with 3 protrusions were made, the next set of samples with 5 protrusions welded simultaneously were made. In order to be able to comparatively analyze the results of the two different situations, new sets of welded test specimens with 3 protrusions but using only one pair of electrodes (Fig. 4.11a) were performed and then, under similar conditions, a new set of welded test specimens with 5 protrusions was performed, for which the same values of the welding regime were kept (Fig. 4.11b).



a) b)

Fig. 4.11*. Images during the experimental program of welding samples with optimized regimes. a) with 3 projections; b) with 5 projections.*

As can be seen from Fig. 4.12, this time, a device for positioning and fixing the specimens during welding was designed and realized, which does not allow their displacement or shifting during weld spot formation.



a)

b)

Fig. 4.12*. Device designed for welding of specimens by resistance relief welding: (a) without specimens; (b) with welded specimens.*

b)

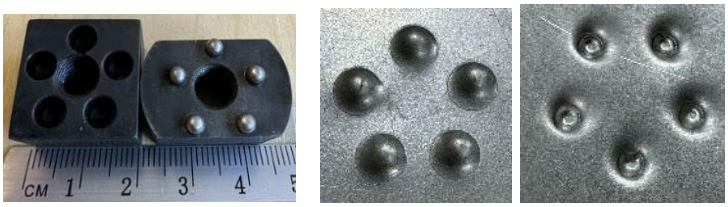
4.2. Experimental investigations of 5-point relief welding of thin components made of aluminized steel

4.2.1. Materials used

The same types of materials used in Chap. 4.1, i.e. aluminized rolled mild steel with thicknesses of 0.8- and 1.2-mm. Strips with a width of 35 mm and a length of 150 mm were cut to make the welded specimens.

4.2.1. Preparation of samples for welding

Starting from the results obtained in the first part of the experimental program, samples were designed and obtained with 5 projections (protrusions). For this, a mold with 5 projections was designed and realized. The dimensions of the protrusions were: height 1.55±0.1mm and diameter at the base 5±0.1mm (Fig. 4.13) and only the strips of the base material were embossed with a thickness of 1.2mm. The protrusions were arranged equidistantly in a circle with a diameter of about 13±0.1mm. Prior to welding, the samples were cleaned and dried to remove contaminants from the cold stamping process.



a) b)

Fig. 4.13*. Sheet metal embossing die (a) and the appearance/arrangement of protrusions on the aluminized sheet metal blank (b).*

4.2.3 Welding of samples with 5 protrusions

For welding, the thinner specimen was placed on the bottom electrode and the thicker specimen, with protrusions facing the bottom plate, was placed on top of it (Fig. 4.14). The actual dimensions of the protrusions made on the 1.2 mm thick component are shown in Table 4.2. The protrusions were embossed on the thicker (1.2 mm) component to ensure better resistance to the hot plastic deformation that occurs during welding. If the hot strength of the material is reduced, the weld spots tend to collapse more quickly during rapid heating under the resistive effect of electric current, becoming flat before the molten core is formed. Because of this, the ultimate strength of the welded joints can be significantly reduced.

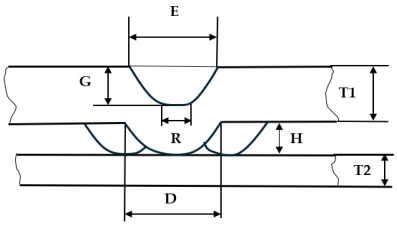


Fig. 4.14*. Layout of the projection welding composites.*

Table 4.2. Projection dimensions* [mm]

No. projections	T1/ T2	G	D	H	E	R
3	1,2 / 0,8	2	4	1,60	4,20	1,5
5	1,2 / 0,8	2,3	5,6	1,80	5,8	2

*Measuring accuracy± 0,01mm

The same TECNA 8005D series TECNA machine (Fig. 4.15) and the pair of copper electrodes with flat surface were used for welding the samples, but different values of the welding regime parameters were chosen (Table 4.2).

The samples also overlapped over a length of 52 mm. This time, strips without a bent edge were used, without the use of a special guiding device, which resulted in a slight de-axis (rotation relative to the axis of the fixed part) when welding. In this set of samples, for a group of 2 or 3 workpieces, only the value of one parameter of the welding regime was changed, while all other parameters were kept equal.

Welding parameters have different effects on the diameter of the weld spot, the degree of expansion of the ZIT, the depth of the footprint that forms above the weld spot, the diameter of the footprint and the degree of material thickness reduction in the weld zone [144-148, 152]. Therefore, the results obtained in the previous experimental program, when welded specimens with 3 protrusions were made (Table 4.3, Fig. 4.16), were considered when determining the values of the welding parameters. The value of the pressing time was kept constant (10 ms) but the welding time was varied (from 5 to 7 ms), while the power had values from a minimum of 17.7 kVA to a maximum of 20.5 kVA.

The electrode pressure had different values, adapted to the values of the electrical parameters. Samples with high pressure values (4 - 5 bar) as well as samples with low and medium values (2.8

bar respectively 3,4 bar). The electrode pressure for carbon steel/soft regime is recommended to be in the range of (7-12) daN/mm^{2}and the pressing force F in the range of (50 - 250) t, i.e. minimum 60 - 300 daN [171]. The range of values chosen for the welding regime parameters used in the final set of 3- or 5-protrusion specimens was determined by optimization with the Taguchi method. The upper and lower limits of the ranges of values for the 3 welding parameters (Power, welding time and pressing force) were established based on the previous tests, to ensure the design requirements of the orthogonal array of factors influencing the welding regime.

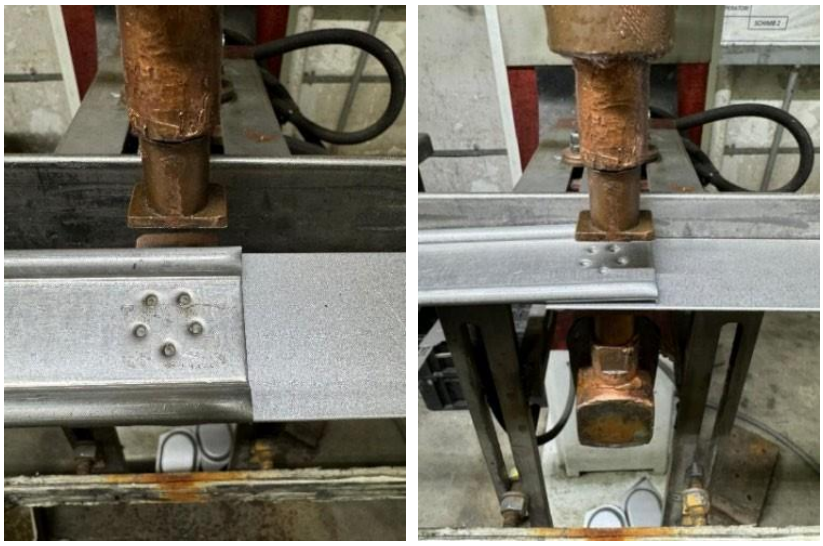


Fig. 4.15 Performing projection welding of specimens with 5 protrusions.

Table 4.3. Welding regime parameters for the 5-protrusion sample set

Sample	SET	Electrode pressure, bar	Time pressing time, ms	Welding time, ms	Welding power, kVA
0.1	0	5	10	7	19,5
0.2		4	10	7	19,5
1.1	1	2,8	10	5	19
1.2		2,8	10	7	19,6
1.3		2,8	10	5	20,5
2.1	2	3,4	10	5	17,7
2.2		3,4	10	7	19,4
2.3		3,4	10	7	17,8
3.1	3	2,8	10	5	19,4
3.2		2,8	10	5	18,9
3.3		2,8	10	5	20,5

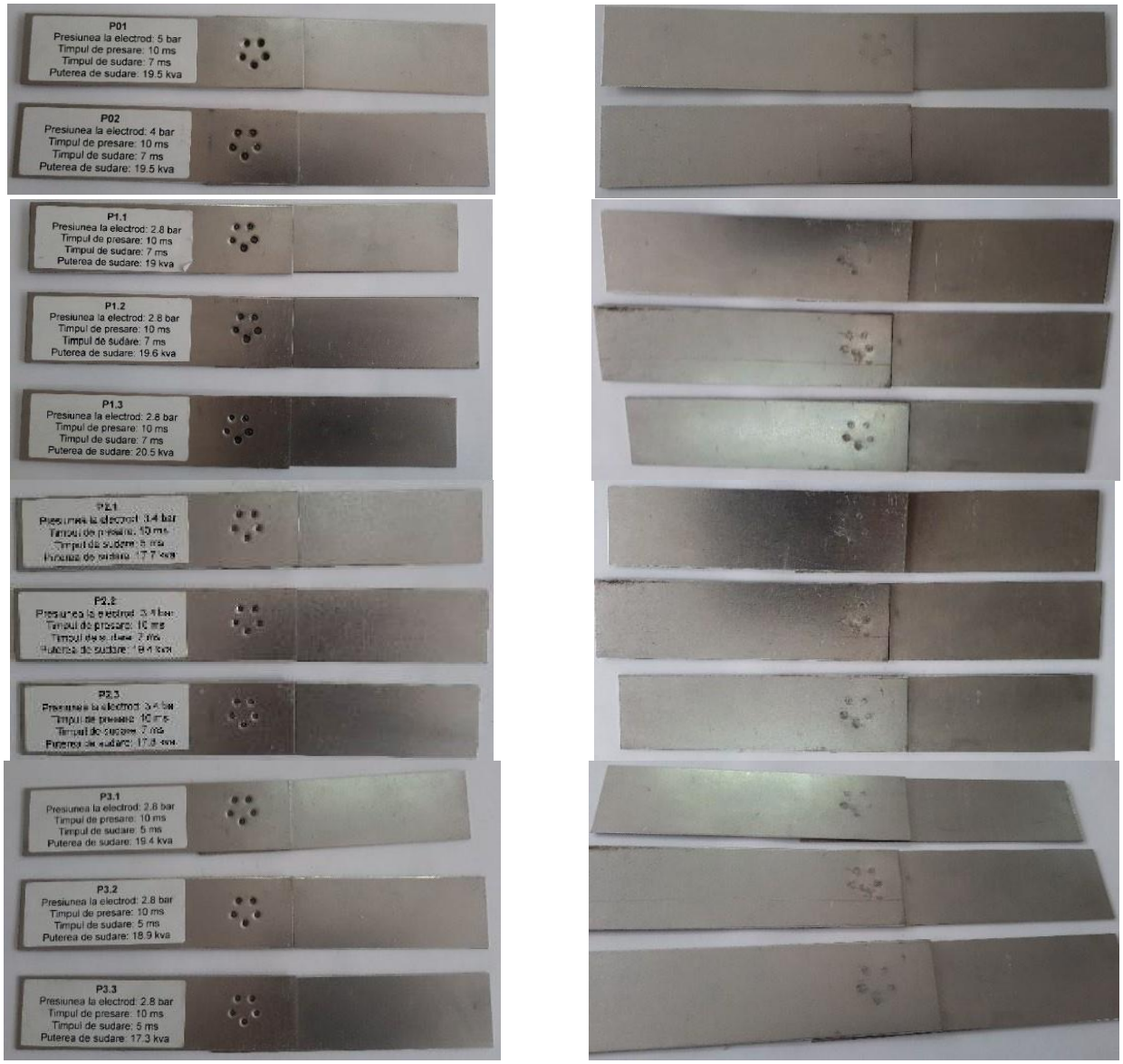


Fig. 4.16*. Third set of 5-protrusion (front/back) relief welded specimens.*

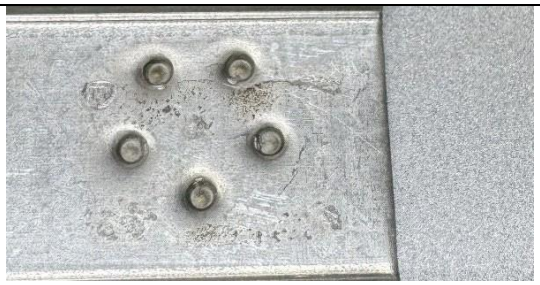
Standard EN 1993-1-3 [173] recommends certain values for the length of resistance spot welded parts or the overlap length. If the diameter of a welded spot is ds=3mm, then the value of the overlap area must be at least 5ds, i.e. 15mm. Since the welded points are distributed at a distance of about 10mm, it follows that the minimum distance required should be 25mm. Therefore, in the experimental program, an overlap of 32- 35mm was achieved for both the 3-protrusion and the 5-protrusion set of boards.

4.3. Welding imperfections

After welding, the samples were visually examined using a magnifier with 5x magnification and a 100-lux lamp. The main types of imperfections identified in the set of 3- and 5-protrusion welded specimens are shown in Table 4.4.

Table 4.4. Types of imperfections identified after projection welding

VISUAL EXAMINATION - *SR EN ISO 17637* - Non-destructive examination of fusion welded joints. Identified imperfections: surface imperfections; Sensitivity of the method: imperfections greater than 0,1 mm; Features: detection by naked eye or with optical devices (magnification up to 10x);	 Impressions too deep, incorrect positioning of punches during impression and electrodes during welding
On some welded samples, imperfections such as oxide deposits or oxide crusts were identified that had detached from the surfaces of previously welded parts and then adhered to the weld surface. These imperfections contribute to worsening heat transfer conditions during welding. Therefore, periodic cleaning of the welding electrode surfaces with fine abrasive papers is recommended.	 Oxide deposits or crusts on component surfaces
Formation of welded spots of different sizes - occurs if the components are not well aligned and positioned, or when the indentations have been made incorrectly, because of wear phenomena occurring on the forming devices, if the electrode surface is loaded with deposits detached from the surfaces of the parts.	  Welded points of different sizes
Loading of the active electrode surfaces with successive layers of aluminum, detached from the aluminized sheets, leads to the formation of inhomogeneous unevenness, which worsens the current transmission through the components during welding, which is detrimental to the appearance and quality of the welded spots or may lead to the formation of incomplete welds.	 Wear spots on the electrode surface

The surface of the electrodes is loaded with different residues of materials deposited from other welded parts or their surface is not smooth/clean. Different filler materials may imprint or adhere to the surface of the welded parts, resulting in an unsightly appearance, partially perforating the protective layer or causing small craters that favor preferential corrosion phenomena.	 Scratches and spots on the surface of welded parts

The characteristics that were considered in the evaluation of resistance welded joints were: a) **weld spot shape** or **fused zone size**, which is defined as the width of the weld spot at the joint interface in the longitudinal direction. This geometrical aspect is the most important factor in determining the quality of electrical resistance spot welds [152]. The size of the fused areas, which determines the total bonding area of the joint, is controlled by the linear energy introduced at sweat (fig. 4.17).



Fig. 4.17*. Weld spot diameter measurement.*

b) **Depth of the indentation of the molten zone in the thickness direction** - can affect the mechanical properties of welds. It depends on the pressure applied to the electrode and the temperature of the electrode/plate interface. Increasing the amount of heat causes the temperature of the interface to increase, which in turn increases the amount of plastic deformation that occurs at the surfaces under electrode pressure. In order to keep the indentation depth to a minimum, the welding parameters and the electrode geometry/surface should be checked before welding.

c) **shape of the notch** at the sheet/board interface: since a notch form along the circumference of the welded spot when welding in relief, the values of the welding parameters must be adjusted so that it is not too obvious. The shape of the notch, whether sharp or square, can affect the breaking behavior of welds (Fig. 4.18).

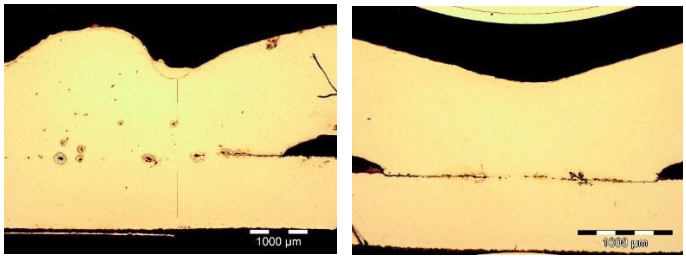


a) 3 protrusions *b) 5 protrusions*

Fig. 4.18*. Appearance of the notches around the welded spots when welding in relief.*

d) **The presence of voids in the molten zone** at the interface between the surfaces of the parts: there are two causes of voids in the weld spots: expulsion of molten metal and solidification

shrinkage (Fig. 4.19).



a) b)

Fig. 4.19*. Imperfections on the weld interface: a) voids; b) lack of adhesion.*

e) **ZIT extension** - the thermally influenced zone, may have a different distribution if parts of different thicknesses are welded, as was the case in the experimental program. The extent of the ZIT depends on the amount of welding energy and the thermal conductivity of the welded materials. Since out-of-equilibrium structures (e.g. martensite) can form when steels cool rapidly, the hardness increases in this zone and the plasticity of the material decreases.

f) **Partially welded and detached spots** - occur if the amount of heat required to form the weld spot has not been correctly localized/dosed (Fig. 4.20).

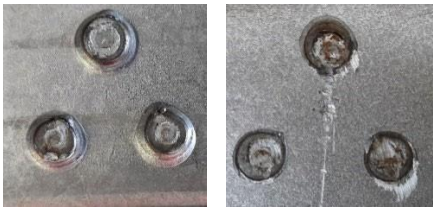


Fig. 4.20*. Partially welded and detached spots in tensile test.*

g) **localization at the welded interface of intermetallic compounds** of high hardness and brittleness, with the development of cracks - accumulation and expulsion of intermetallic compounds occurred because the welded sheets were coated with a thin layer of Al-Si alloy from the manufacturing process.

Chapter 5 CHARACTERIZATION AND TESTING OF WELDED SPECIMENS BY ELECTRICAL RESISTANCE PROJECTION WELDING

5.1 Microscopic analysis

5.1.1. Base material analysis

Optical analysis of the microstructure of the aluminized steel surface revealed the formation of alpha-aluminum dendrites and interdendritic compounds between alloying elements (Fig. 5.1a). According to the EDS analysis performed on the surface of the aluminized steel sheet (Fig. 5.1b), the chemical composition contains (wt.%): 79.31 Al; 11.96 Si; 2.04 Fe; 0.34 Cr; 0.40 Ca; 5.96 O. Elements such as Ca and O may also originate from the working atmosphere in which the

samples were exposed for about 6 months of operation. The evolution of the concentration of the main chemical elements in the vicinity of the aluminized layer (Fig. 5.1b) indicates a lower concentration of aluminum at the outer surface (consumed for the formation of aluminum oxide and Al-Si compound), then it increases in the middle zone of the aluminized layer, after which it starts to decrease towards the interface with the steel sheet. At the same time, the diffusion of iron towards the aluminized layer is also observed, with the formation of the hard compound Al-Fe [41, 130-131].

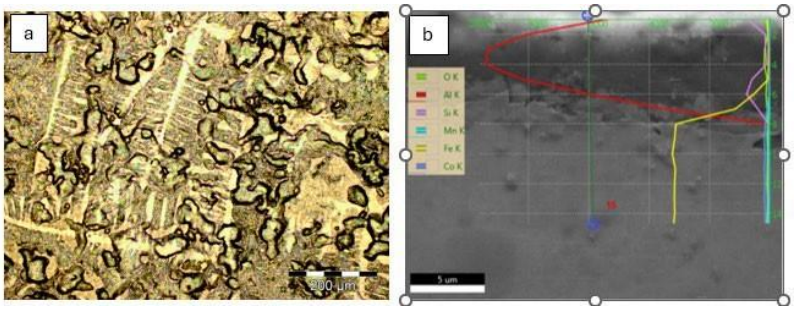


Fig. 5.1. *Analysis of the microstructure and chemical elements present at the surface of aluminized steel. a) appearance of the aluminized surface; b) distribution analysis of the chemical elements along the interface between the aluminized layer and the base metal (cold-rolled non-alloy steel).*

The SEM analysis performed on the surface of the aluminized sheet showed a quasi-uniform appearance of the aluminized layer (discontinuous film, dendritic in appearance, with a variable thickness of about 20µm) (Fig. 5.2). The chemical composition analysis revealed the presence of aluminum as the major element (more than 79% Al), together with Oxygen from aluminum oxide (5.96%), Si (11.96%), Fe (2.04%) and residual elements Ca (0.4%) and Cr (0.34%). In the detailed cross-sectional image of sample 1.1 (Fig. 5.2), the structure of the aluminized layer is visible, which is composed of a thin adhesion layer, SA (about 5microns thick) located at the interface with the steel component and the Al-Si (AL) alloy layer (about 20 microns thick).

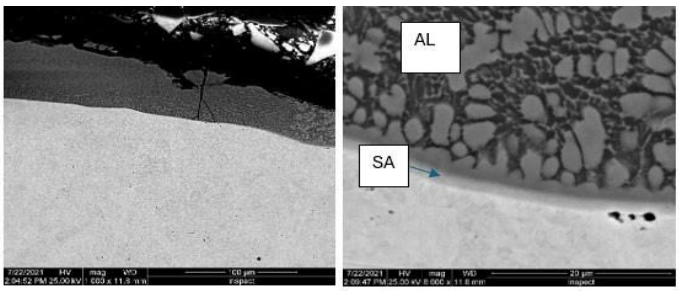


Fig. 5.2. *Cross-sectional image through the base material and detail in the aluminized layer existing on the steel surface [59, 63].*

In the base material (steel), at a short distance from the bonding layer, the chemical composition contains (mass %): 1.22% Al; 0.94% Si; 96.29% Fe; 1% Co; 0.54% Cu. The analysis of the chemical composition on either side of the interface between the aluminized layer and the steel sheet is shown in Fig. 5.3. At about 15 µm from the interface (Spot 1 and Spot 2), the chemical composition in the aluminized layer contains between 30-31%Al, 3.5 - 3.75%Si, 0.3-2.57 %Mn and 62-65%Fe.

5.1.1. Analysis of welded specimens with 3 projections

To study the effects of welding parameters on the weld spot geometry and the change in coating thickness, cross-sections through the welded spots were realized with different regimes. To study the microstructure and to measure the microhardness on the welded area, cross- sections through the welded spots were performed using the IsoMet 4000 high precision cutting machine. The microstructural analysis was performed by optical microscopy using the Olympus GX51 microscope equipped with specialized image processing software (AnalySIS) and by scanning electron microscopy using the Inspect S microscope equipped with the AMETEC EDAX Z2e EDAX AMETEC sensor for micro chemical composition analysis on restricted areas. In order to highlight the effect of the welding regime on the weld zone geometry and the continuity of the protective oxide layer, cross-sections through the welded spots were performed (Fig. 5.5). Using AnalySIS software, the values of the height of the peak and recess zones, respectively, which are formed during plastic deformation of the material during welding (H, H1, H2), as well as the values of the apparent diameter of the weld spot (D) were measured.

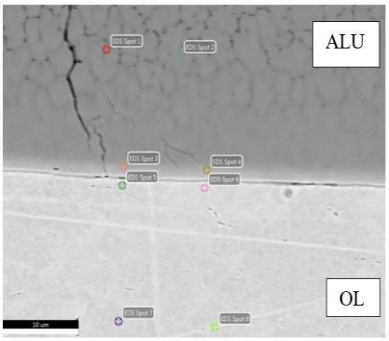


Fig. 5.3 *Location of chemical composition measurement points at the interface between the aluminized layer (ALU) and the steel sheet (OL)*

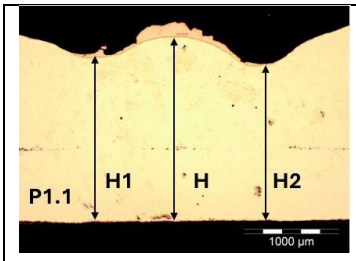


a) b) c)

Fig. 5.4. *Resin embedded samples prepared for metallographic analysis:*
a) Sample 1.1, set II; b) Sample 1.2, set I; c) Sample 2.2., set I.

In sample 1.1, although the power value was lower than in sample 1.2 (18.08 kVA vs. 19.18 kVA), for identical values of welding and pressing time, the breakage occurred at a higher

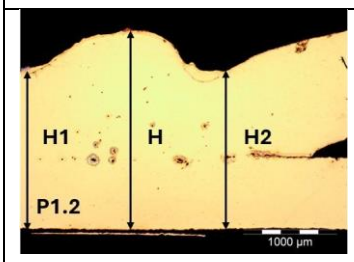
value (13.764 kN vs. 11.738 kN), because the welding clamping pressure was higher (2.8 bar vs. 2.6 bar). The stronger pressing of the material on the protrusion allowed the formation of a larger diameter point, which had a better breaking strength than the similar sample analyzed. In addition, because the energy supplied to the weld was lower, the fused zone had better resistance to deformation (collapse) during the formation of the weld spot. In comparison with sample 2.2, where the welding power and pressing time had nearly equal values, increasing the welding pressure value (from 2.8 bar to 3.4 bar) did not result in an improvement of the breaking strength. Failure occurred at a force value of only 11.455kN. Although a lower welding power value was chosen (Test 1.1/set II, 18.08kVA) but a higher welding time value (7msec), the Al-Si protective layer deformed and cracked, causing a localized thickening at the tip of the weld spot, with a thickness of about 160 µm (Fig. 5.6).



a. P1.1/set II

Presiunea la electrod, bar	Timpul de presare, ms	Timpul de sudare, ms	Puterea la sudare, kVA
2,8	10	7	18,08

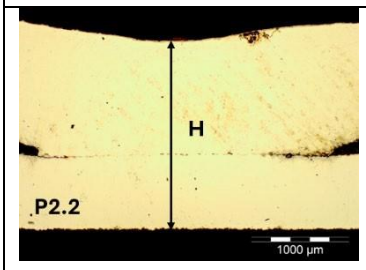
Breaking force = **13,764 kN**
Displacement at break = 10,114 mm
Location of break= base material



b. P1.2/set I

Presiunea la electrod, bar	Timpul de presare, ms	Timpul de sudare, ms	Puterea la sudare, kVA
2,6	10	7	19,18

Breaking force = **11,738 kN**
Displacement at break = 7,3984mm
Location of break= base material

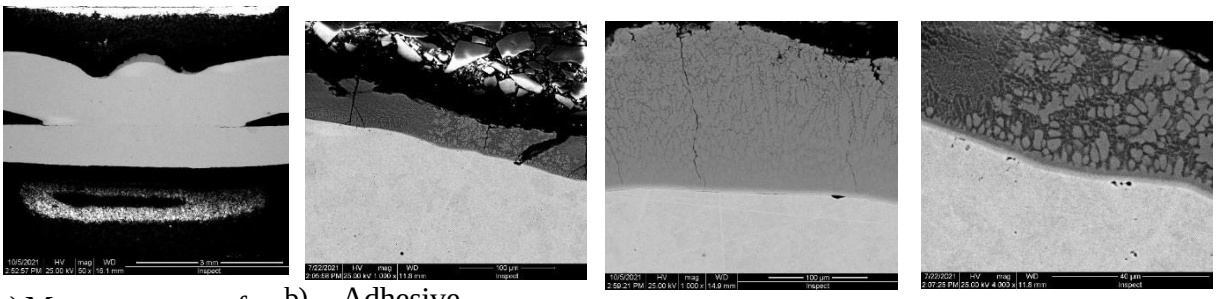


c. P2.2/set I

Presiunea la electrod, bar	Timpul de presare, ms	Timpul de sudare, ms	Puterea la sudare, kVA
3,4	10	5	18,10

Breaking force = **11,455 kN**
Displacement at break = 6,106 mm
Location of break= weld spot

Fig. 5.5*. Cross-sections of 3-protrusion relief welded specimens*



a) Macrostructure of the weld spot

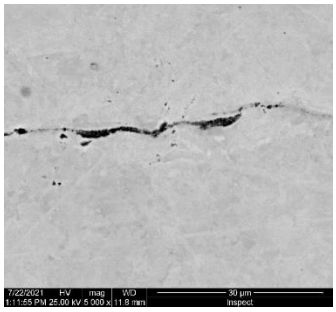
b) Adhesive aluminized layer with cracks

c) Detail on the aluminized layer area

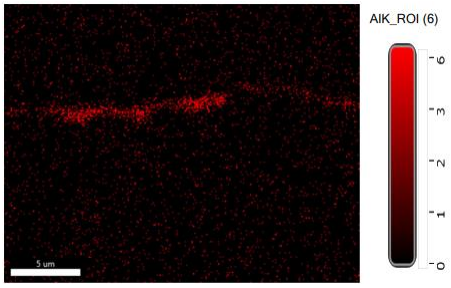
d) Dendritic structure of the aluminized layer

Fig. 5.6*. Weld spot analysis in cross section for sample 1.1, set 1I.*

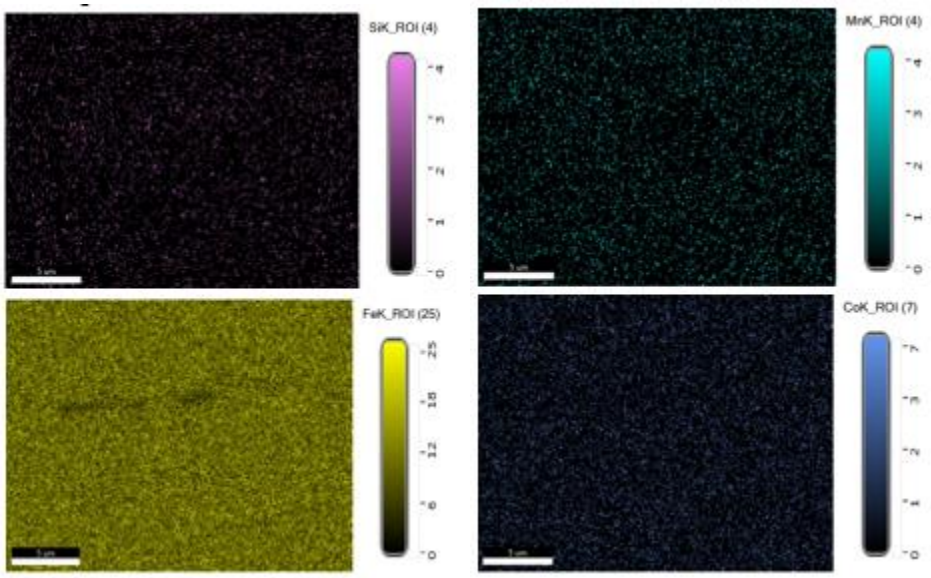
During welding, the fragments resulting from the breaking of the AlSi layer together with the reaction compounds formed with impurities on the workpiece surfaces were largely expelled to the lateral areas of the weld (Fig. 5.7) because of the pressure exerted by the electrodes.



a) Analysis area of the interface between the welded components

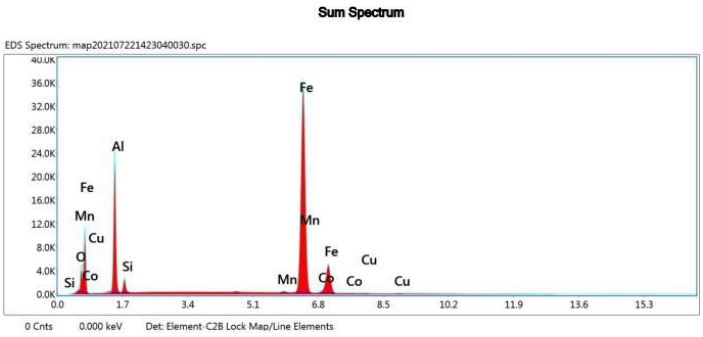


b) EDAX image of selected area a zonei selectate pentru analiza



5.7. *Lenticular, chained, lenticular compounds sprinkled on the fusion line of the weld spot and images of the atomic distribution of the elements on the selected area. Sample 1.1, Set 2(b).*

From the chemical element distribution images shown in Fig. 5.7, Al-rich dendritic formations (deep red color) and compounds formed withFe, Si or Cu are observed. Global analysis of the chemical composition (mass percentages) by diffraction using the EDAX method indicates values of more than 25% for Al, more than 70% for Fe and more than 2.6% Si.Small concentrations of Co are derived from the parent material (Fig. 5.8).



Smart Quant Results

Element	Weight %	Atomic %	Net Int.	Error %	Kratio	Z	A	F
O K	0.38	1.01	8.61	14.31	0.0015	1.2049	0.3295	1.0000
AlK	25.61	40.51	833.84	7.70	0.0919	1.0881	0.3294	1.0014
SiK	2.60	3.94	90.31	8.67	0.0097	1.1146	0.3330	1.0024
MnK	0.29	0.23	11.39	17.93	0.0030	0.9432	0.9870	1.1190
FeK	70.23	53.67	2288.00	1.20	0.6734	0.9600	0.9949	1.0039
CoK	0.75	0.54	21.52	12.82	0.0070	0.9400	0.9839	1.0067
CuK	0.14	0.09	2.88	41.70	0.0012	0.9268	0.8988	1.0156

Fig. 5.8 *Global chemical composition analysis for selected micro-array (Radiation Intensity versus Energy, keV)*

From Fig. 5.9, which shows the evolution of the concentration of chemical elements along a line crossing the welded interface, the abundance in the aluminized coating of Al and Si, as well as the diffusion of Fe, Mn and Co elements from
(surface of the steel piece towards the crust).

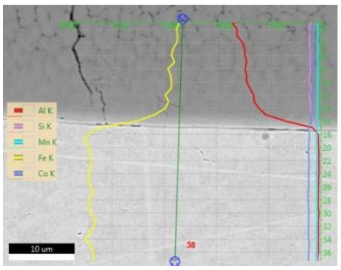


Fig. 5.9*. Distribution of the chemical elements across the interface between the Al-Si oxide crust and the welded steel component.*

Due to the stresses arising from hot deformation followed by sudden cooling during welding, cracks frequently appear in the oxide-embedded layer, which propagate and stop at the steel surface (Fig. 5.10).

These cracks increase the risk of detachability of the protective layer and allow the penetration of the working medium, causing surface corrosion. In the case of sample 1.2, the aluminized layer did not undergo very large changes in thickness compared to sample 1.1. Increasing the welding power (from 18.08 to 19.18kVA), reducing the electrode pressure (2.6bar) and maintaining the same welding time (5 msec), resulted in better continuity and more uniform thickness of the aluminized layer.

However, thickness irregularity and small buildups (indicated by arrows) can be observed on the marginal (micro-crater) areas of the weld spot (Fig. 5.11), localized in the deformation zone of the protrusion. In this sample, on the weld interface (LF - line of fusion) there are elongated inclinations with larger dimensions than those observed in sample 1.1.

The presence of the intermetallic compounds was due to the welding regime, which did not allow their expulsion, the total cross-section of the spot being even smaller (2.6 compared to 3.12mm measured in sample 1.1).

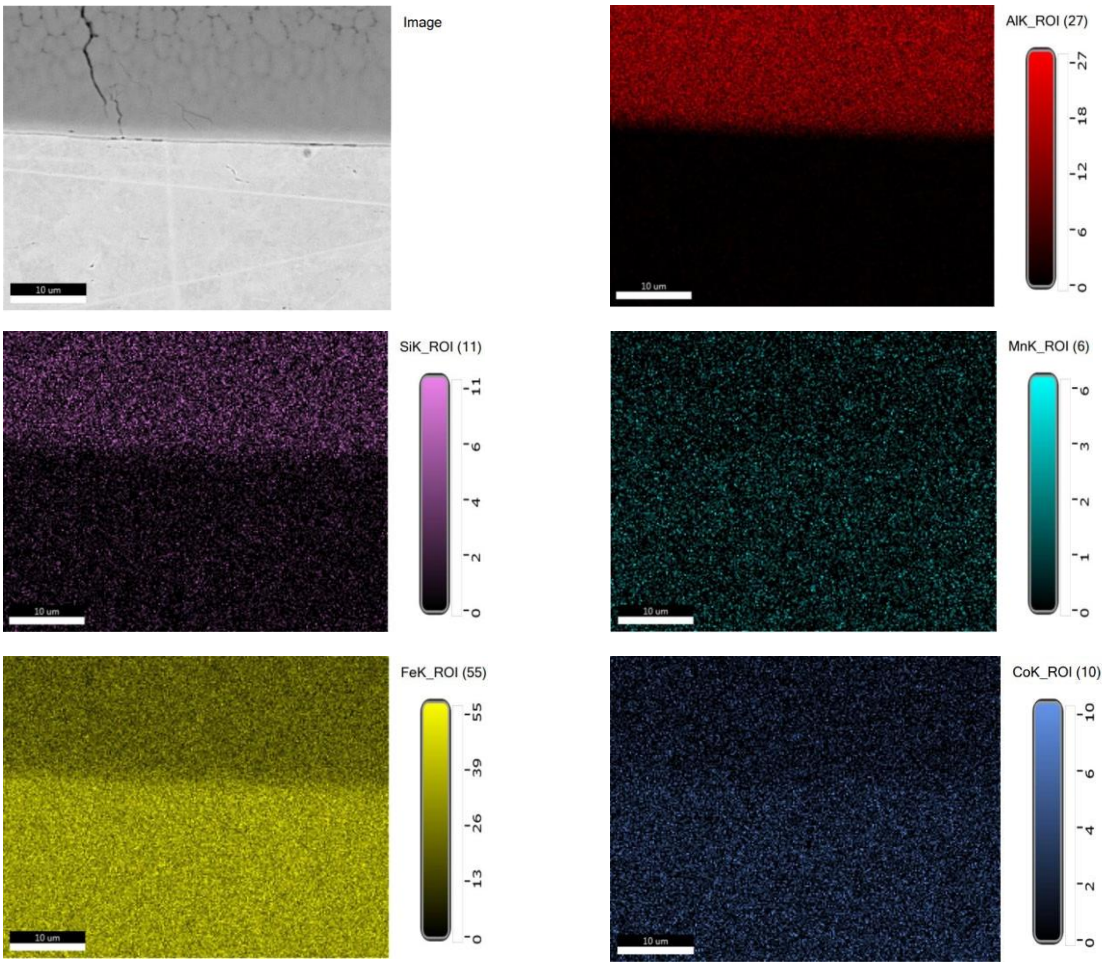


***Fig. 5.10**. Atomic distribution images of the chemical elements at the interface between the welded part and the oxide crust formed on its upper surface (sample 1.1 set 2).*

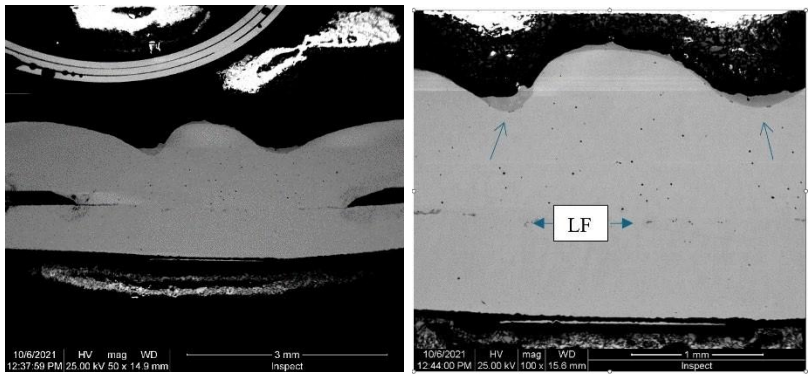


***Fig. 5.11.** Detail on the weld spot area of sample 1.2./set 1 showing the accumulation of compounds detached from the aluminized layer.*

Detailed analysis on the interface zone with the aluminized layer for sample 1.2 is shown in Fig. 5.12. The data presented in Fig. 5.12 indicate the decrease in Al concentration (mass percent) from the maximum value of more than 88% (Spot 1, aluminized layer surface) to 1.11% in the steel substrate (about 20 microns below the welded interface). The average Al concentration was obtained at about 2microns from the fusion line in the aluminized layer, after which the concentration of this element decreased drastically to 1%. The Si content was also reduced from a maximum of 6.66% in the upper areas of the aluminized layer to 0.92-1% in the areas close to the welded interface. The compounds formed at the interface of the molten core of the welded spot have different chemical compositions, depending on the degree of mixing and the reaction rate of the elements, under the very high welding and solidification rates specific to the process studied. The reaction compounds formed on the interface of the fusion line in Sample 1.2, Set 1 have high concentrations of Al and Si (18% Al and 2.78% Si in Spot 1, 15.75% Al and 2.66% Si in Spot 2, respectively 17.5% Al and 7.84% Si in Spot 5).

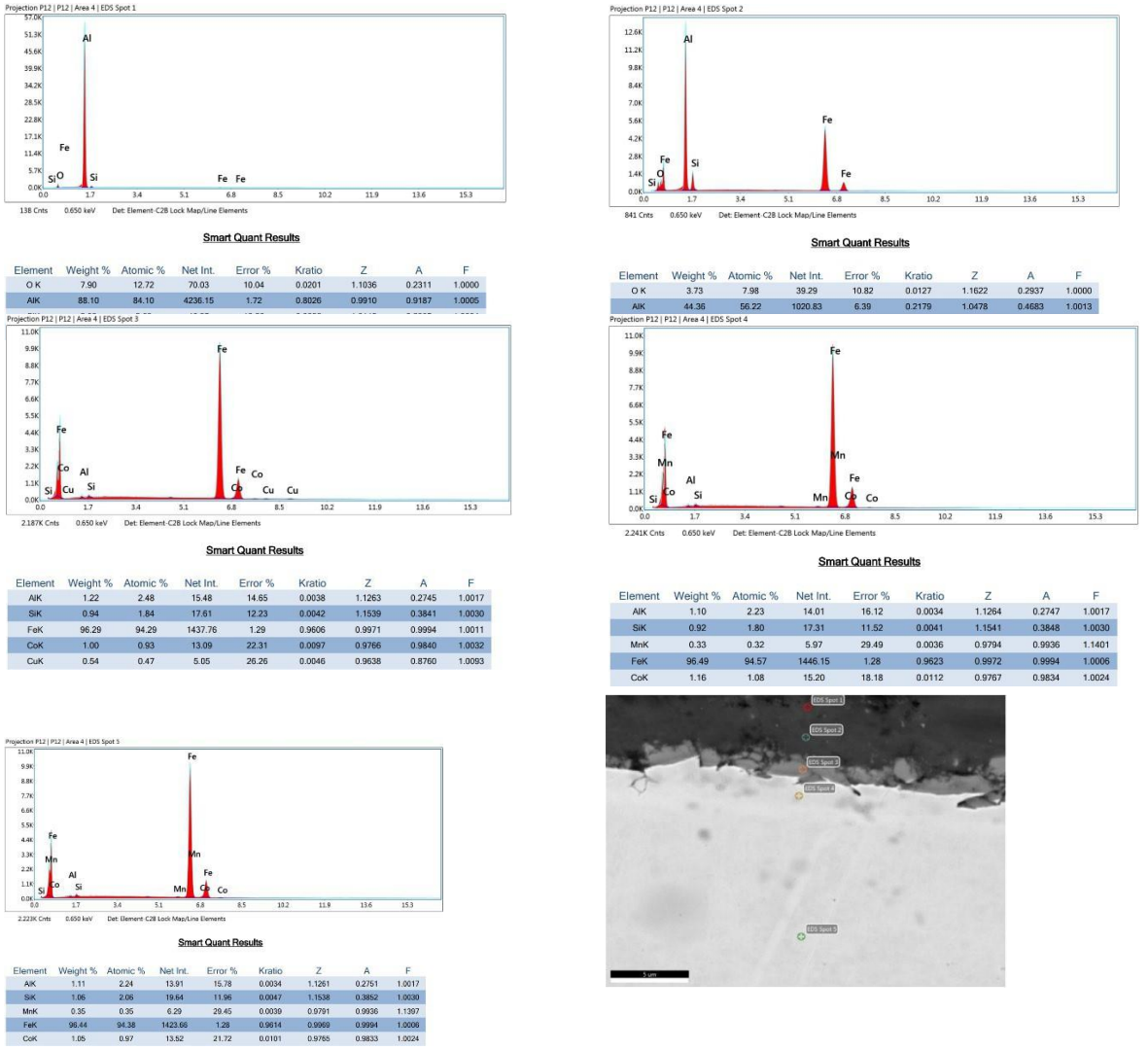
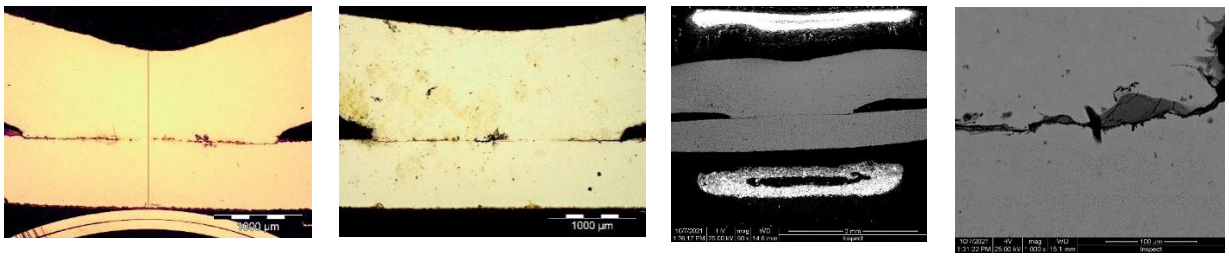


Fig. 5.12. *Quantitative analysis of chemical microcomposition on the areas adjacent to the aluminized layer for sample 1.2/set 1 (Radiation Intensity versus Energy, keV).*

Sample 2.2 (Fig. 5.13) has a completely different appearance from the other samples presented above, as it no longer shows the specific annular area of protrusion deformation on the weld spot surface, but only a slight flattening of the protrusion. The cumulative total length of the weld spot diameter is the smallest, only 1.52mm.



a b c d

Fig. 5.13*. Highlight of the marginal areas of the weld spot with inclusions accumulations in the case of the sample*
2.2/set 1. Optical microscopy (a) and SEM electron microscopy images (b, overall view of the welded area; c) detail on the area at the surface end of the weld spot where the build-up of compounds is observed).

5.2 Burst testing

To evaluate the shear strength of the welded spots, the samples were subjected to the continuous tensile test. Single point shear stress can be calculated using the relation:

$$\tau = \frac{4F}{\pi D^2} \quad (5.$$

where F is the breaking force and D is the diameter of the weld spot.

The values of τ for specimen 1.1 was 208.7 MPa, for specimen 1.2 was 183.2MPa and for sample 2.2 was 103.2MPa.

Test specimens were 32 mm wide and 150 mm long. Three protrusions of the same dimensions (depth and diameter) were made on each of these samples. When welded, an overlap of 32 mm length was made. The test conditions were:

- test speed: 5mm/min ->10mm, 10mm/min ->20mm, 20mm/min ->60mm
- distance between trays: 147mm
- data acquisition rate: 0,001/s

Images of welded parts during continuous tensile stress are shown in Fig. 5.14. Using the integrated data processing program with which the tensile testing machine is equipped, displacement acquisitions (during plastic deformation and solid-state flow) were made with increasing tensile force value, which are plotted cumulatively as stress versus strain curves (Hooke plots). Continuous tensile test evolution curves (Hooke plots) were also plotted for each welded specimen (Fig. 5.15). Specimens in which the fracture is localized in the base material and in which the value of the fracture force is greater than or at most equal to that of the base material are considered good.

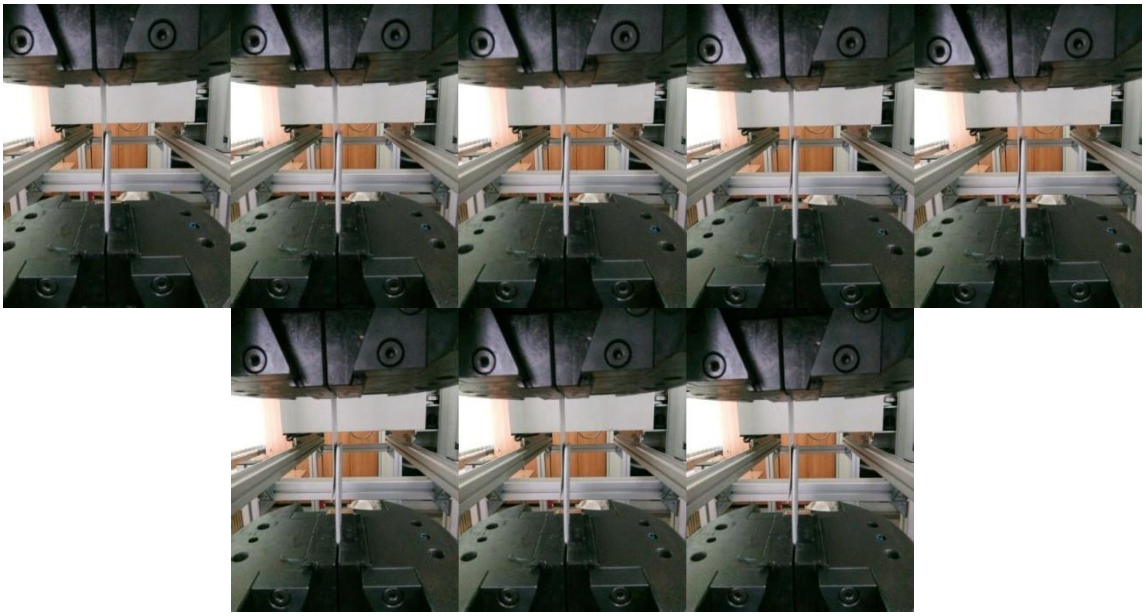


Fig.5.14 *Behavior of welded parts during tensile stress.*

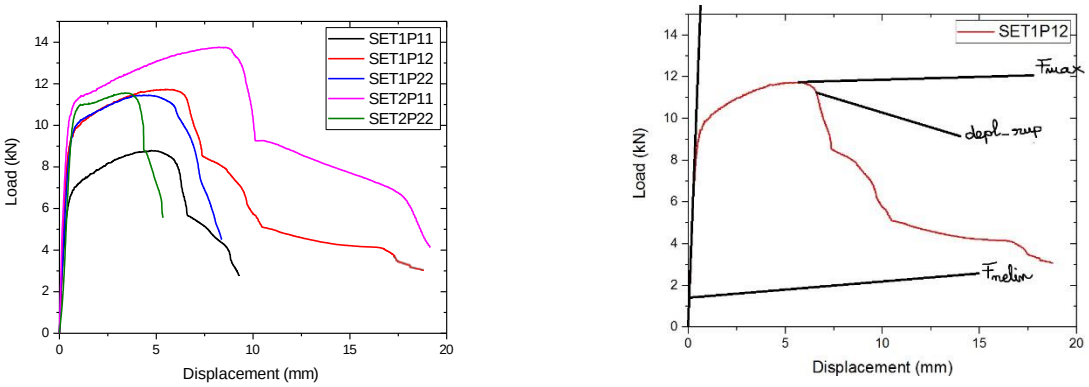


Fig. ***5.15*** *Cumulative Hooke - Load - Displacement diagrams for the welded sample set (a) and explanations of representative areas of the Hooke diagram (b).Fnelin - nonlinear force; Fmax - maximum force, depl-rup - displacement at rupture.*

5.2.1 Tensile test results for welded specimens with 3 protrusions

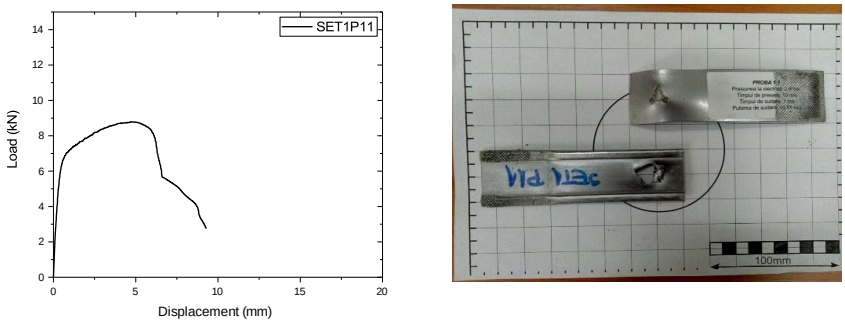


Fig. 5.16 *Hooke diagram and appearance of specimen P1.1, SET I, after rupture. Fracture occurred at a maximum force of 8,789kN, with failure of the base material.*

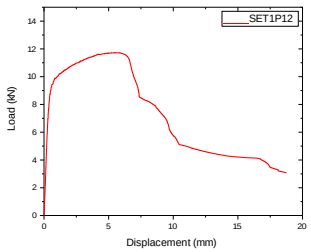




Fig. 5.17 *Hooke diagram and appearance of specimen P12, SET1 after rupture. Fracture occurred at a maximum force of 11.738kN with failure of the base material.*

The actual values of forces and displacements recorded for the welded specimen sets are given in Table 5.1.

Table 5.1. Tensile test results for 3-protrusion welded relief specimens

Code Sample	Set	Fmax [kN]	F nelin [kN]	Displacement at break [mm]
P1.1	SET1	**8,789**	2,1843	6,6149
P1.2	SET1	11,738	1,2933	7,3984
P2.2	SET1	11,455	2,2005	6,106
P1.1/2	SET2	**13,764**	4,5396	10,114
P2.2/2	SET2	11,557	4,8762	4,3574

From the analysis of the results of the continuous tensile test the highest breaking force value was obtained for P1.1/set 2. Localized imperfections in the weld melt line caused premature failure of some welded joints during operation at temperatures between 180-200$^{(o)C.}$ During welding, in the melted core, the protective layer of aluminum alloy was first melted and then solidified rapidly.

5.2.2 Tensile test results for welded specimens with 5 protrusions

For the batch of 5-protrusion specimens, the test conditions were like those established for the batch of 3-protrusion welded specimens. The values of the test parameters in the tensile test are given in Table 5.2. For easier interpretation of the results and to study the effects of the welding parameters on the tensile strengths, the Hooke diagrams of the 4 sets of welded specimens were plotted cumulatively.

Table 5.2. Tensile test results for 5-protrusion relief welded specimens

Code Sample	Stiffness [kN/mm]	Fmax [kN]	Fracture		Energy consumed [kN*mm]
			Force [kN]	Displacement [mm]	
P0.1	35,335	16,56	16,553	3,7054	53,91
P0.2	32,948	15,956	15,738	3,6037	50,38
P1.1	32,076	16,246	16,081	3,8674	53,39

P1.2	33,446	16,282	16,243	5,042	72,71
P1.3	31,401	16,342	16,168	4,4323	62,67
P2.1	31,257	14,946	14,9	1,8215	21,73
P2.2	32,561	16,075	16,005	4,163	57,89
P2.3	30,812	14,448	13,557	2,1532	25,34
P3.1	31,936	15,177	15,032	2,4794	31,75
P3.2	31,783	15,636	15,217	2,7246	33,16
P3.3	31,735	14,831	14,29	1,827	17,58

Figure 5.18 shows the stress/strain diagram for the two welded specimens P01 and P02. Figure 5.19 shows the Hooke diagrams for the set of specimens P1.1, P1.2 and P1.3. 5.26 shows the Hooke diagrams for the set of samples P3.1, P3.2 and P3.3.

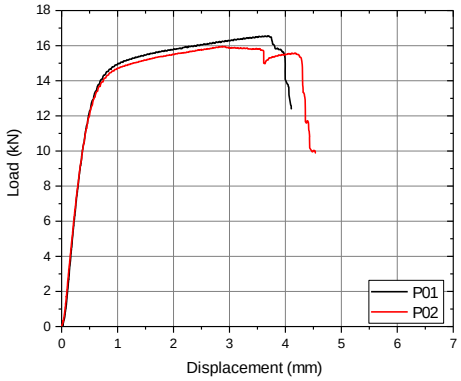


Fig. 5.18 *Hooke diagram for samples P01 and P02. The failure occurred first in sample P02 at F = 15.738kN, while sample P01 failed at F= 16.553kN.*

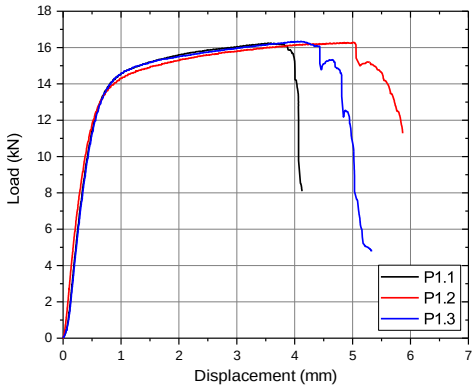


Fig. 5.19 *Hooke diagram for samples P1.1, P1.2 and P1.3. The failure occurred first in sample P1.1 at F = 16.081kN, followed by P1.3 which failed at F = 16.168kN*

5.3 Hardness measurements

The experimental determination of microhardness was carried out with Shimadzu HMV 2T equipment under the following working conditions: temperature +25°C (reference temperature +23 ±5°C) and humidity 55%. The microhardness was measured on the cross-section of the welded specimens, applying indentation load of 0.2 N and indentation time of 10s. The values are shown in Table 5. 3.

Table 5.3. Hardness values of 3-protrusion relief welded specimens

Sample/ Measurement area	**Individual values, HV0.2**	**Mean value, HV0.2**	**Deviation Standard**	**Coefficient of variation**
Base material	155, 152, 158, 156, 157	156	2.30	1.48
Sample 1.1				
Aluminized layer	870, 856, 864, 864, 851	861	7.48	0.87
Fusion line	193, 187, 184, 190, 185	188	3.70	1.97

HAZ*	161, 158, 165, 155, 153	158	4.77	3.01
Sample 1.2				
Fusion line	190, 185, 188, 183, 181	185	3.65	1.97
HAZ	160, 152, 160, 158, 155	157	3.46	2.21
Sample 2.2				
Fusion line	178, 170, 179, 178, 176	176	3.63	2.06
HAZ	152, 155, 153, 159, 153	154	2.79	1.81

*HAZ – heat affected zone

Chapter 6 OPTIMIZATION OF THE WELDING PROCESS IN RELIEF

6.1. General aspects

One of the widely used methods to optimize the parameters of processing regimes is the one proposed by Geniki Taguchi [157-159]. With the help of this method, it is possible to eliminate the parameter values that lead to product quality variations during the manufacturing of products. More specifically, this strategy should be developed that allows optimizing the values of the most important process parameters. The process of optimization of the relief welding process has to go through the following stages: Design of the welding system, Design of the technological (measurable) parameters, Establishment of tolerance limits for the parameter values. In order to implement the Taguchi method, the factorial design (the design of the strategy for conducting the experiments) must be established, in which **the input variables** that interact with **the outcome** (output) **factors** are defined, resulting in results with an acceptable level of confidence. The classification of factorial experiments is done with the relation:

$$□=□^{□} \quad (6.1)$$

Where L is the number of levels of each influencing factor, and m is the number of factors of the technological process affecting the quality of the welding process [158-160].

In the case of the welding process analyzed in the PhD thesis there are 4 input influencing factors (F1 - Electrode pressure with values of 2.8 and 3.4; and 5 bar; F2 - Welding time, with values of 4; 5; 6 and 7 ms; F3 - Welding power with values between 17.7; 19; 19.5 and 20.5 kVA; F4 - Pressing time with a single value of 10ms). It results that $N = 4^3 = 64$. Since F4 is single-valued, it will not be introduced in the influence factor matrix. The summarized presentation of the influence factors is given in Table 6.1.

Table 6.1. Factors influencing the electrical resistance relief welding process

Parameter	**Symbol (units of measurement**	**Levels of influencing factors**			
		F1	**F2**	**F3**	**F4**
Welding power	Ps (kVA)	17,7	19	19,5	20,5
Welding time	*t* (ms)	4	5	6	7
Electrode pressure	*P* (bar)	2,8	3,4	4	5

In the case of the welding process analyzed in the PhD thesis there are 4 input influencing factors (F1 - Electrode pressure with values of 2,8; 3,4; 4 and 5 bar; F2 - Welding time of 4,

5; 6 and 7 ms; F3 - Welding power with values between 17,7; 19; 19,5 and 20,5 kVA; F4 - Pressing time with a single value of 10ms). Since F4 has a single value, it will not be introduced in the influence factor matrix. Applying the input data in equation 6.1, it follows that a minimum of N
= 4^3= 64 experiments. The concept of "robust parameter", introduced by Genichi Taguchi, aims to design a design of experiments, in which the interaction between the control variables and the uncontrollable deviation is analyzed, which is achieved by control factor settings that minimize the variation in the response of the uncontrolled factors [158]. To evaluate the significance of process parameters, Taguchi method uses a statistical measure of performance called signal-to-noise (S/Z) ratio, which considers both the mean value of the values and their variability. The S/Z ratio is the ratio of the mean value (signal) to the standard deviation (noise), depending on the quality characteristics of the product/process to be optimized. The standard S/Z ratios commonly used are: nominal-is-best (NB), smallest-is-better (MicB) and largest-is-better (MareB).

6.2. Making welded specimens according to the optimized experimental plan

Based on the input data, we proceeded to the **second phase of** the optimization methodology.

First, strips of material (aluminized steel with thicknesses of 0.8mm and 1.2mm), 40mm wide and 150mm long, were cut using a guillotine cutter. Then, the 1.2mm thick samples were indented, 16 samples with 3 protrusions and 16 samples with 5protrusions, respectively. The dimensions of the protrusions area are schematized in Fig. 6.1 and the measured values are centralized in Table 6.2
.

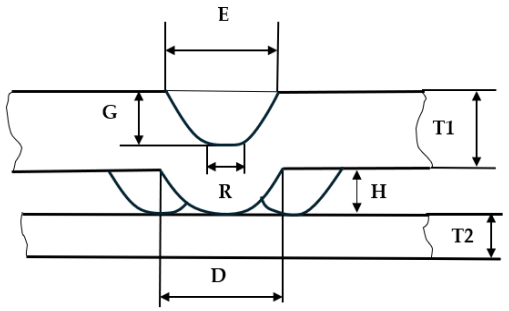


***Fig. 6.1**. Protrusion measurement scheme.*

Table 6.2. Calculated/measured dimensions of protrusions* [mm]

Number of projections	T1	T2	G	D	H	E	R
3	1,2	0,8	2	5	2	2,6	1.5
5	1,2	0,8	2,3	5,4	2.3	3	2

* Measuring accuracy± 0.01mm; **D is determined with the formula: D=E+2xT1;

The welded samples were then performed as 2 sets, one set of 16 welded samples with 3 protrusions and one set of 16 welded samples with 5 protrusions (Fig. 6.2). For all welded specimens the same value of pressing time of 10ms was kept.

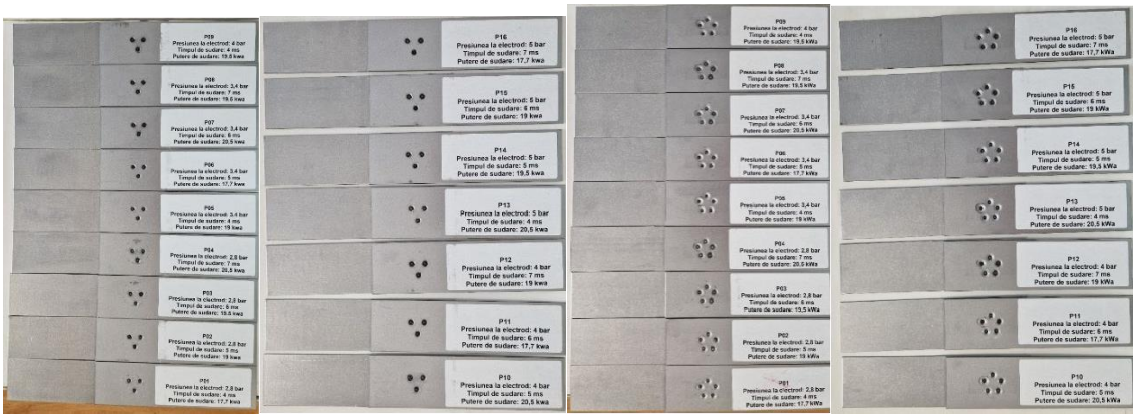


Fig. 6.2*. Set of 3- and 5-protrusion resistance welded specimens*

.

6.3. Destructive testing of welded specimens

The welded specimens were then subjected to the continuous shear test, using the same apparatus as that used for the specimens analyzed in Chapter 5. The results obtained in the point shear shear test for the set of welded specimens with 3 protrusions made in the optimization procedure are shown in Table 6.3.

Table 6.3. Detailed experimental design for set I (3 protrusions)

No. exp.	Parameters			Response		
	Pressure, *Pr*, bar	**Time, *T*, ms**	**Power, *P*, kWA**	**Maximum breaking force F_r, kN**	**Displacement during rupture D_r, mm**	**Location/ Breaking mode**
1	**2,8**	**4**	**17,7**	**8,5851**	**1,5323**	Base material
2	2,8	5	19	10,723	2,9071	Base material
3	2,8	6	19,5	10,535	2,7287	Base material
4	2,8	7	20,5	10,680	2,4025	Basic material
5	3,4	4	19	10,202	2,8863	Base material
6	3,4	5	17,7	10,941	3,022	Base material
7	3,4	6	20,5	10,772	2,9455	Base material
8	3,4	7	19,5	10,904	3,0986	Base material
9	4	4	19,5	10,924	3,3854	Base material
10	4	5	20,5	10,782	3,299	Basic material
11	**4**	**6**	**17,7**	**11,033**	**3,1994**	Basic material
12	4	7	19	10,944	3,08	Basic material
13	5	4	20,5	10,964	3,1621	Base material
14	5	5	19,5	10,984	3,3373	Base material
15	5	6	19	10,805	3,1982	Base material
16	5	7	17,7	10,901	3,265	Base material

From Table 6.3, it can be seen that the average value of the strain at break for the welded specimen set with 3 protrusions is about **2.86** mm. In Table 6.3, the limiting situations, i.e. the weakest specimen and the best specimen tested, have been highlighted. The graphical representation of stress-strain curves for set I (optimized) 3-projection welded relief specimens is shown cumulatively (Fig. 6.3 and Fig. 6.4). The required diameter of a point is given by the relation D= 4t. In this case, it is certain to break the component with the smallest thickness, t=0.8mm.

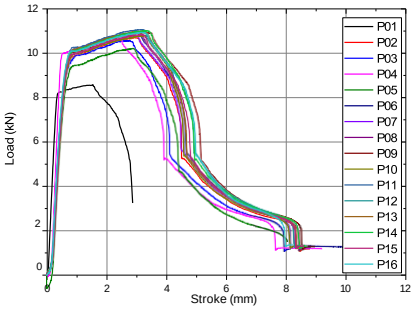


***Fig. 6.3**. Stress-strain curves in the continuous rupture test for the I -optimized set of 3-protrusion welded relief specimens.*

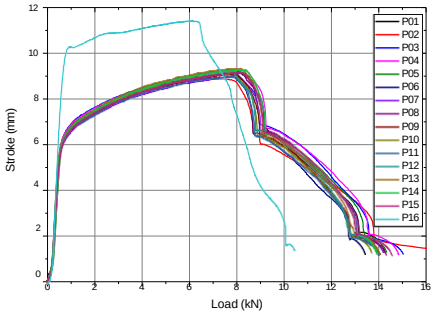


***Fig. 6.4** Cumulative stress-strain curves at continuous rupture test for the optimized set II of 5-protrusion relief welded specimens.*

Table 6.4. Detailed experimental plan for set II of specimens (5 projections)

No. experiment.	Parameters			Response		
	Pressure, *Pr*, bar	Time *t* ms	Power, *P*, kWA	Maximum breaking force F_r, kN	Displacement during rupture D_r, mm	Mode/cycle breaking
1	**2,8**	**4**	**17,7**	9,1656	7,9475	Base material
2	2,8	5	19	**8,8854**	7,2448	Base material
3	2,8	6	19,5	9,156	7,745	Basic material
4	2,8	7	20,5	9,2385	8,0252	Base material
5	3,4	4	19	9,1857	8,1314	Basic material
6	3,4	5	17,7	9,1032	7,4998	Base material
7	3,4	6	20,5	9,0174	7,9234	Base material
8	3,4	7	19,5	9,1857	8,0537	Base material
9	4	4	19,5	9,0933	7,9519	Base material
10	4	5	20,5	9,1692	7,8556	Base material
11	4	6	17,7	8,991	7,7833	Base material
12	4	7	19	9,2319	7,6202	Base material
13	5	4	20,5	9,3375	8,0887	Base material
14	5	5	19,5	9,2715	**8,3984**	Base material
15	5	6	19	9,156	8,22	Basic material
16	**5**	**7**	**17,7**	**11,406**	6,1885	Basic material

Chapter 7 CONTRIBUTIONS AND CONCLUSIONS. DIRECTIONS FOR FURTHER RESEARCH

7.1. GENERAL CONCLUSIONS

The desk study that has been carried out in the first part of the PhD thesis has allowed us to draw some conclusions related to the particularities of the electrical resistance relief welding process, as follows:

1. A basic requirement in relief welding is the ability to quickly break or remove the oxide layer or coating from the surface of the parts, so as to ensure a good mechanical contact and hence correct electrical contact between the two base materials.
2. Destructive testing methods also include tensile strength testing, exfoliation testing, shear testing, corrosion resistance testing, optical or electron microscopy analysis on cross-sections of the welded joint, chemical micro-composition analysis on fusion zones, etc.
3. Variations in thickness, tensile strength, hardness, as well as the degree of surface finish or degree of cleanliness of the parts being welded have a significant effect on weld quality.
4. Rapid hardening in electric resistance welding can lead to hardening and embrittlement effects in non-alloy steels with higher carbon and manganese content, as a result of the occurrence of martensite and bainite microstructures.

Conclusions from the experimental welding of thin aluminized steel components

1. During welding, the protective AlSi alloy layer fragments, melts and gives rise to reaction compounds together with impurities on the surfaces of the workpiece. This is finally expelled to the lateral areas of the weld (Fig. 5.7) because of the pressure exerted by the electrodes during welding.
2. The very high hardness value of the aluminized layer above the weld spot (861 HV0.2) is due to the formation of hard Al-Fe compounds, as iron diffuses from the steel sheet during welding. Chemical composition measurements on the micro-area adjacent to the aluminum layer determined a concentration of 2% Fe.
3. Imperfections that were observed on the weld melt line contributed to the premature failure of the welded joints during operation at temperatures between 180- $200^{(o)}$ C. The aluminum alloy protective layer underwent changes during the welding process, melted and then solidified rapidly, generating the shrinkage stresses that caused cracking/rupture of the protective layer, which allowed the unprotected areas to be exposed to the action of the working environment (hot oil, steam, temperatures of about 180-$200^{o)}$ C.
4. The breaking surfaces of the 3 welded spots have different shapes and areas, due to the wear of the electrode surface (the pressing is uneven at the 3 spots, deformation of the plates during pressing or incorrect positioning, as well as due to the thermal imbalance occurring when the electric current passes through the aluminized steel.
5. The optimum values of the welding regime parameters for the 5-protrusion specimens were: electrode pressure 2.8 bar, welding type 7ms and power 19.6 kVA. In this case, the values of the tensile breaking forces (16.553 kN) are 20% higher than those obtained for the 3-protrusion specimens, i.e. Fmax= 13.674 kN.

7.2.1. *Theoretical contributions*

- Documentation of the particularities of the electric resistance relief welding process in order to develop the experimental program;
- Analysis of the effects of the protective layers on the surfaces of the welded specimens on the weld spot formation mechanism
- Design of an experimental program for obtaining and testing of 3 and 5 protrusion relief welded specimens; Identification of the influencing factors on the welding process, analysis of the stress conditions of the welded products, identification of disturbing factors (current fluctuations, measuring limits of the equipment used, wear of the welding equipment, pressure losses in the hydraulic pressing system, etc.) in order to optimize the values of the welding regime parameters.

7.2.2. *Scientific contributions*

- Design of the technology of electric resistance welding of components of different thickness (0.8 and 1.2 mm respectively) made of aluminized steel; Design of the technological documentation for the manufacture of welded parts with the electric resistance welding process, design and realization of a device for positioning the welded samples; Realization of 4 sets of 16 welded samples with different welding parameters for 3 and 5 projections.
- Development and realization of an experimental program of destructive testing of welded samples, study of the mode of breakage and analysis of parameter values: Breaking force, deformation at break; Carrying out an extensive microstructural characterization of the welded spots in the experimental program, using optical microscopy, SEM scanning electron microscopy, Study of the diffusion phenomena of chemical elements coming from the aluminized layer through the welded interface, local chemical micro-composition analysis with the EDAX method, identification of microstructural changes, phases and metallographic constituents, highlighting the diffusion phenomena of chemical elements through the interface of the welded deposition;
- Design and execution of a large program for optimization of the welding regime parameter values using the Taguchi method.

Selective bibliography

1. Larsson J.K., Bengtsson L., "The Overlooked Joining Technology of Fasteners for Modern Car Body Structures - Latest Experience From Nut and Bolt Attachment to Advanced High Strength Steels," in proceedings from 11th European Automotive Engineers' Council (EAEC), Budapest, May-June **2007**.
2. O'Brien R.L., Welding Handbook: Welding Processes (Miami: American Welding Society, **1991**, II, pp. 562-563.
3. Tolf E.G., Hedegard J, "Resistance Nut Welding: Weldability to Ultra High Strength Steels and Joint Properties," in proceedings from 59th Annual Assembly of IIW (International Institute of Welding), Quebec, August-September **2006**.
4. R. Khezri, Static Strength of Weld Nuts on Carbon and Boron Sheet Steels, report IM-2007-104, Stockholm: KIMAB - Corrosion and Metals Research Institute, March **2007**.

5. J.W. Ringsberg, P. Orvegren, H.F. Henrysson, and G. Kerstrm, "Sheet Metal Fatigue Near Nuts Welded to Thin Sheet Structures in Car Bodies," proceedings from FATIGUE 2006 - 9th International Fatigue Congress, Atlanta, May **2006**.
6. Voiculescu, I., **Oprea, A.V**., Vasile, I.M., Case Study About Resistance Projection Welding of Aluminized Steel Parts, .Annals of "Dunarea de Jos" University of Galati Fascicle XII, Welding Equipment and Technology, Vol. 32, p. 23-29, **2021**. **DOI:** https://doi.org/10.35219/awet.2021.03, cited by Mikno, Z. Analysis of projection welding in relation to the non-parallelism of electrodes. *Int J Adv Manuf Technol* **135**, 2087-2095 (2024). https://doi.org/10.1007/s00170-024-14653-x
7. **Oprea, A.V**, Ciocoiu, R. C., Vasile, I.M. Lala, C. G., Geanta, V., Voiculescu, I., Study about multipoint projection welding of aluminized steel plates, VIII International Congress "Engineering, Environment and Materials in Process Industry ",Bosnia, Febr**. 2023**.
8. **Oprea, A.V,** "Research on the effect of electric resistance relief welding regime parameters on the ultimate tensile strength of steel components", Welding Conference, Cluj, April 7-8**, 2022**.
9. Goral, M.; Pytel, M.; Ochal, K.; Drajewicz, M.; Kubaszek, T.; Simka, W.; Nieuzyla, L. Microstructure of Aluminide Coatings Modified by Pt, Pd, Zr and Hf Formed in Low-Activity CVD Process. Coatings, **2021**, 11, 421. https://doi.org/10.3390/ coatings11040421
10. **Oprea, A.V.,** Voiculescu, I., Simulation of the projection welding process, DIGITAL 4PPP Workshop, Nov. 24, **2023**, Bucharest, Romania.
11. **Oprea, A.V.**, Vasile, I. M., Ciocoiu, R.C., Voiculescu, I., The Effect of Protrusions Number at Projection Welding Process, International Conf. Bramat, **2024**, Brasov, Romania, poster.
12. **Oprea, A.V.**, Vasile I. M., Voiculescu I., Ciocoiu R. C., The Multipoint Relief Projection Study, PriMera Scientific Engineering, Volume 3 Issue 1, July **2023**, ISSN: 2834-2550, doi:10.56831/PSEN-03-061, https://primerascientific.com/pdf/psen/PSEN-03-061.pdf.
13. **Oprea, A.V.,** Voiculescu, I., Ciocoiu, R.C., Vasile, I.M., Research Regarding Multi-Point Projection Welding Process, Conf. ICMaS, 2023, 16. Nov, Bucharest, Romania.
14. Wang Min Wang, Welding methods of aluminized steel pipe, Journal of Tool & Equipment and Engineering, **2003** (153): 47-48.
15. Patel, N.; Parihar, P.L.; Makwana, J.S. Parametric Optimization to Improve the Machining Process by Using Taguchi Method: A Review. *Materials Today: Proceedings* **2021**, *47*, 2709-2714.
16. Wang, X., Zhang, Y., Effects of Welding Procedures on Resistance Projection Welding of Nuts to Sheets, ISIJ International **2017**, Vol. 57 No. 12, pp. 2194-2200.
17. Mathiszik, Ch., Johannes Koal, J., Zschetzsche, J., Füssel U., Schmale H.C., Study on precise weld diameter validations by comparing destructive testing methods in resistance spot welding, Welding in the World (**2024**) 68:1825-1835 https://doi.org/10.1007/s40194-024-01747-z.
18. Sherepenko, O.; Kazemi, O.; Rosemann, P.; Wilke, M.; Halle, T.; Jüttner, S. Transient Softening at the Fusion Boundary of Resistance Spot Welds: A Phase Field Simulation and Experimental Investigations for Al-Si-coated 22MnB5. Metals **2019**, DOI: 10.13140/RG.2.2.32009.93280
19. Wang, X., Zhang, Y., Effects of Welding Procedures on Resistance Projection Welding of Nuts to Sheets, ISIJ International **2017**, Vol. 57 No. 12, pp. 2194-2200.
20. **Oprea A. V.,** Ciocoiu R. C., Constantin G., Voiculescu I., Optimization of Parameters in Multi-Spot Projection Welding of Thin Aluminized Steel Sheets, APPLIED SCIENCES-BASEL, Volume 15, Issue 19, DOI 10.3390/app151910530, Article Number 10530, Published SEP 29 2025,Indexed2025-10-20, WOS:001593458800001, eISSN 2076-3417